Effect of Solution-Hardening on the Evolution of Nanostructure in Ni-Fe alloys during Severe Plastic Deformation by High Pressure Torsion

Nida Khan

A Dissertation Submitted to

Indian Institute of Technology Hyderabad

In Partial Fulfillment of the Requirements for

The Degree of Master of Technology

भारतीय प्रौद्योगिकी संस्थान हैदराबाद

Indian Institute of Technology Hyderabad

Department of Materials Science and Metallurgical Engineering

July, 2014

Declaration

I declare that this written submission represents my ideas in my own words, and where others' ideas or words have been included, I have adequately cited and referenced the original sources. I also declare that I have adhered to all principles of academic honesty and integrity and have not misrepresented or fabricated or falsified any idea/data/fact/source in my submission. I understand that any violation of the above will be a cause for disciplinary action by the Institute and can also evoke penal action from the sources that have thus not been properly cited, or from whom proper permission has not been taken when needed.
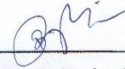
<div align="right">

Nida.

_____
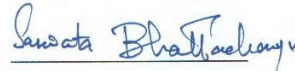
(Signature)

Nida Khan

MS12M1008

</div>

Approval Sheet

This thesis entitled "Effect of Solution-Hardening on the Evolution of Nanostructure in Ni-Fe alloys during Severe Plastic Deformation by High Pressure Torsion" by Nida Khan is approved for the degree of Master of Technology from IIT Hyderabad.
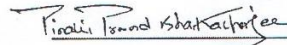
Dr. B. Panigrahi
Department of Materials Science and Metallurgical Engineering
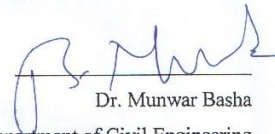Examiner

Dr. Saswata Bhattacharya
Department of Materials Science and Metallurgical Engineering
Examiner

Dr. Pinaki Prasad Bhattacharjee
Department of Materials Science and Metallurgical Engineering
Adviser

Dr. Munwar Basha
Department of Civil Engineering
Chairman

Acknowledgements

Dedicated to

My Parents

Abstract

Solid solution hardening via alloying addition could be used to control the microstructure, texture and properties of a range of alloys. However, solution-hardening due to alloying should be generally accompanied by change in stacking fault energy (SFE).Thus, the evolution of microstructure and microtexture during severe plastic deformation (SPD) could be affected by both solution-hardening and change in SFE. However, the extent of their individual effect should be isolated for better understanding of these parameters.

In the present work Ni-Fe alloys were studied as a model system to evaluate the effect of solid solution hardening on microstructure and texture evolution during SPD processing by High Pressure Torsion (HPT). This alloys system was particularly suitable for the present study as alloying of Fe with Ni resulted in solution-hardening but no significant change in the SFE. A series of Ni-Fe alloys with composition Ni-10%Fe, Ni-20%Fe and Ni-30%Fe were SPD processed by HPT at room temperature to different number of rotations (N), namely, N=1/12, 1/4, 1/8, 1/2, 1, 3, 5 and 10 under an applied load of 5GPa. It was observed that homogenous equiaxed microstructure with grain size ~160 nm and large fraction of high angle boundaries (~80%) are achieved in both Ni-20%Fe and Ni-30%Fe after 10 revolutions but hardness value(~ 470Hv) was uniform throughout the disk only in Ni-30%Fe after 10 whole revolutions. The microtexture of these alloys were found to be similar indicating that texture evolution was not significantly influenced by solid-solution hardening. A comparison with a series of Ni-Co alloys (where the SFE was decreased systematically with alloying addition) obtained from previous studies revealed that increased solution-hardening was also an equally effective strategy as decreasing SFE in achieving nanostructure during SPD processing.

Nomenclature

SPD-Severe Plastic Deformation

UFG-Ultra Fine Grained Material

HPT-High Pressure Torsion

N-Number of Rotations

SFE –Stacking Fault Energy

FCC-Face Center Cubic

ECAP-Equal Channel Angular Pressing

ARB-Accumulate Roll Bonding

BNM-Bulk Nanostructured Materials

EDM –Electric Discharge Machine

XRD-X-ray Diffraction

FEG-SEM- Field Emission Gun equipped Scanning Electron Microscope

EBSD-Electron Back Scattered Diffraction

Θ_{mis} -Misorientation Angle

HAGBs-High Angle Grain Boundaries

LAGBs-Low Angle Grain Boundaries

Θ-Shear Direction

R-Radial Direction

Z-Shear Plane Normal

Hv-Vicker's Hardness

GB maps-Grain Boundary Maps

GBCD-Grain Boundary Characters Distribution

PFs-Pole Figures

ODF-Orientation Distribution Function

TBs-Twin Boundaries

Contents

Chapter 1

Introduction

1.1.Overview

1.1.1.Bulk nanostructured materials

Ultrafine and nanocrystalline materials are defined as polycrystalline materials that have at least one dimension in submicron (≤1µm) or "nanoscale" (≤100 nm) [1]. Bulk Nanostructured materials (BNMs) is a general term given to materials containing nanocrystalline grains (<100 nm) where the sample is in bulk shape and size extending to several millimeters [2]. BNMs are particularly attractive as grain size is a key microstructural factor affecting many physical and mechanical properties of polycrystalline materials. As the grain size decreases the strength of the materials increase according to the Hall-Petch relation: $\sigma = \sigma o + C/\sqrt{d}$ where σ is flow stress, σ_o is friction stress, C is constant and d is grain size.

Nanostructured materials can be fabricated by two routes: (1) Bottom-up and (2) Top-down. In bottom up fabrication route, bulk part is formed by agglomeration of individual atom or nanoscale particle. Typical processes generally employed for bottom up route are inert gas condensation, high energy ball milling, electrodeposition, physical vapor deposition, chemical vapor deposition etc. However, some of the major limitation associated with this route are that the bulk

parts produced are either of very small size, having residual porosity and prone to contamination during processing.

In top down route a bulk solid with coarse grain structure is processed so as to refine the grain size up to submicron or nanometer level. Refinement of grain via top down route is achieved by severe plastic deformation (SPD). SPD is a metal forming process in which high strains are imposed on the work-pieces without any significant change in the overall dimensions. SPD processed materials are having ultrafine structures having mainly high angle grain boundaries (HAGBs) [3]. Typical SPD routes are high pressure torsion (HPT), equal channel angular processing (ECAP), cyclic extrusion and compression (CEC), multi-direction forging(MDF), accumulative roll bonding (ARB) repetitive corrugation and straightening (RCS), cyclic closed-die forging (CCDF), super short multi-pass rolling (SSMR) etc. [4]. Schematics of few of the more popular SPD methods are shown in Fig.1.1.
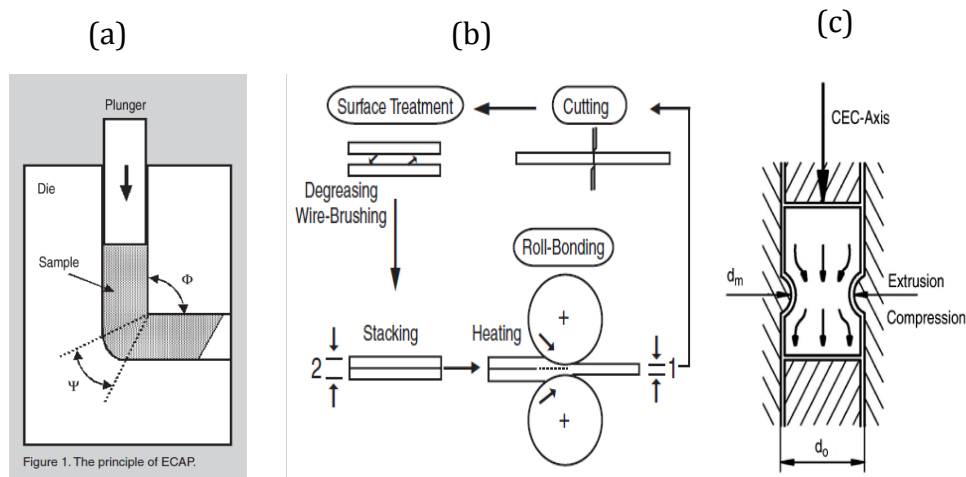
Fig.1.1.Various kinds of SPD processes (a) ECAP, (b) ARB and (c) CEC [1]

1.1.2 High Pressure Torsion

HPT processing was first introduced in 1943 by P. W. Bridgman. Amongst all the SPD techniques HPT is most effective for imposing very large strains even in difficult to deform materials [5]. HPT processing has the ability to routinely produce ultrafine equiaxed microstructure [6]. In HPT processing samples in form of thin disks are placed in between two anvil applying high pressure and torsional strain concurrently. The principle of HPT is shown schematically in the figure below [1].

Fig.1.2.Schematic illustration of HPT [2]

HPT processing can be done in two distinct ways, constrained and unconstrained modes. In constrained HPT there is no outflow of material during. In unconstrained HPT material is free to free to flow outward during processing[2]. The schematics of constrained and unconstrained HPT are shown in Fig.1.3.
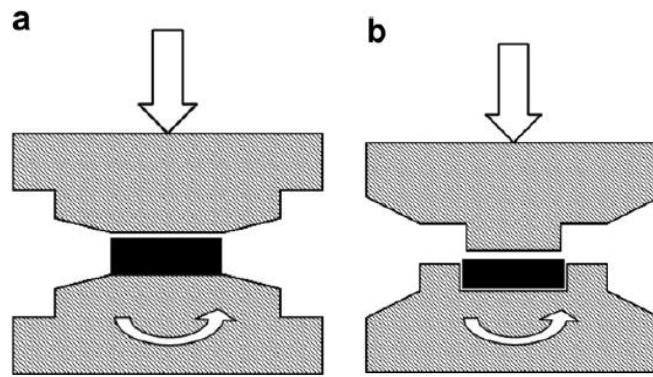
Fig.1.3.(a) Unconstrained HPT (b) Constrained HPT[2]

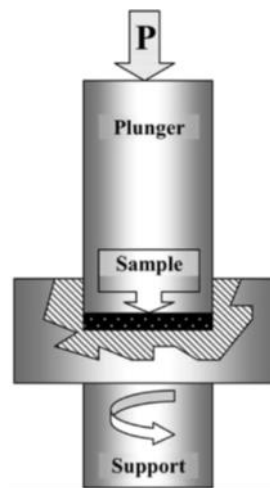### 1.1.3.Strain estimation in HPT processing:

Shear Strain imposed on HPT sample is given by the formula:

$$\gamma = 2\pi N \cdot r/h$$

Equivalent strain can be calculated using the relationship:

$$\varepsilon = \gamma/\sqrt{3}$$

This strain values is correct for small imposed shear strains ($\gamma \geq 0.8$), for larger imposed strains equivalent strain is given by:

$$\varepsilon = (2/\sqrt{3})ln[(1 + \gamma^2/4)^{1/2} + \gamma/2]$$

Where γ = shear strain, ε is equivalent strain, N is No. of revolution, r is radius of disk and h is height of disk

One of the unique features of HPT processing is strain gradient from center of the disk to the edge, as a result of which the microstructure of the HPT sample is

inhomogeneous across the disk. But this heterogeneity in microstructure can be overcome by increasing applied pressure and imposed strain [2]
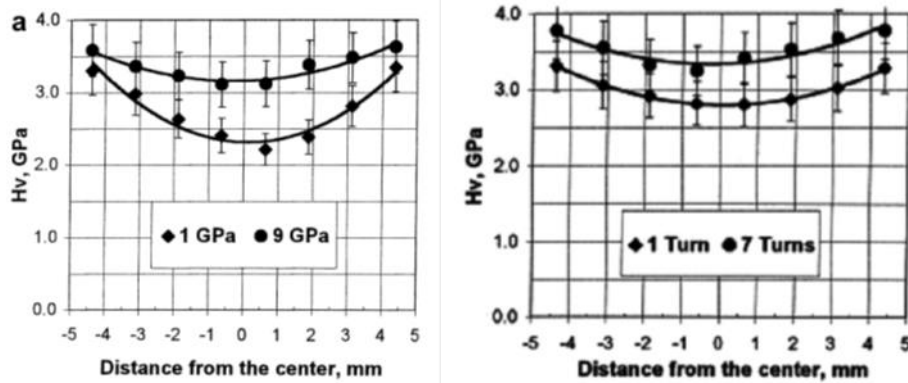
Fig.1.4.Microhardness profiles of nickel processed by HPT at (a) two different applied pressures, the samples were subjected to HPT at room temperature through 5 whole turns (b) two different numbers of whole turns, the samples were subjected to HPT at room temperature with a pressure of 6 GPa[2].

1.2 Objectives of study

Nickel and Iron have similar atomic diameters but different shear modulus so addition of Fe in Ni there is a significant solution hardening effect but there is marginal effect on stacking fault energy (SFE) [7]. Thus the present study on the selected alloy system will be helpful to understand the effectiveness of solution hardening on the evolution of microstructure during severe plastic deformation by HPT.

Fig.1.5.Variation in SFE values of Ni-Fe alloys as a function of Fe concentration

The objectives of the present study are to understand;

The effect of solution hardening on the evolution of microstructure and texture in a series of Ni-Fe alloys during severe plastic deformation by HPT.

Chapter 2

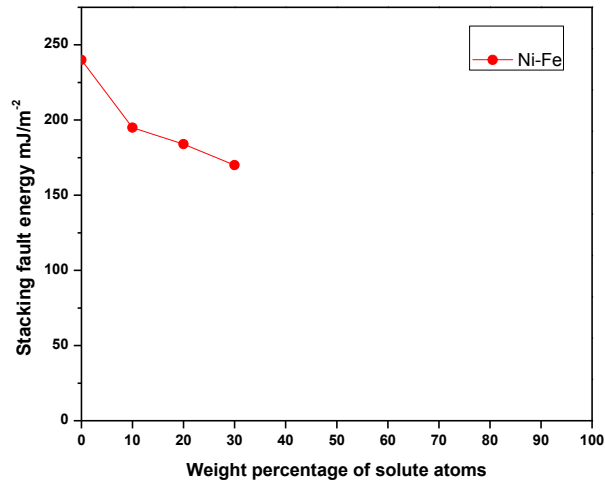# Literature Review

Stacking fault energy (SFE) plays an important role on the evolution of microstructure and texture which is well studied during conventional deformation processing [7]. For example in high SFE materials like high purity aluminum, cross slip and recovery are rather easy. As a consequence heavily deformed microstructure of aluminum shows subgrain structure with sharp subgrain boundaries, whereas, deformed low stacking fault energy materials like austenitic stainless steel, silver etc., reveal typical cell structure with high dislocation density [8]. Thus it is a natural extension that SFE will also affect the evolution of microstructure and texture during deformation by SPD

It might be noted that the change in SFE is significantly affected by alloying. In most cases alloying addition leads to accompanying solution hardening and generally lowers the SFE [10,11,12]. Therefore, alloying also plays a significant role in grain refinement during SPD via its effect on SFE. Minimum grain size at certain temperature can be decreased substantially by alloying, for example at room temperature the grain size of pure Fe, ferritic steel and austenitic steel is 150 nm, 70nm and 30 nm respectively [5]. Alloying in addition to increasing the strength in nanocrystalline materials also enhances some favorable properties, such as, thermal stability [9]. It is thus important to isolate the effect of alloying from SFE to

understand the contribution of solution-hardening on microstructure refinement during SPD.

Zhao et al has studied various Cu-Zn alloy systems processed by HPT and demonstrated various properties and microstructural changes by alloying. When Cu is alloyed with Zn the stacking fault energy decreases with increasing Zn content from 78 to 35 and finally to 14 mJ/m^2 in Copper, bronze and brass, respectively. At the same time grain size is also decreased in the three materials, 84, 54 to 17 nm, respectively [10]. It has also been showed that with decreasing SFE tensile strength and ductility are also improved [11].

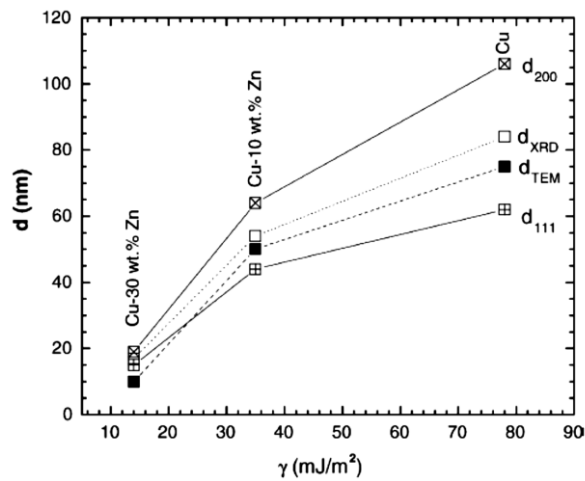**Fig.2.1.XRD-measured grain sizes of Cu and Cu–10 wt. % Zn, Cu–30 wt. % Zn [10]**

Similarly, X. H. An et. al.have investigated microstructural characteristics and strength of plastically deformed Cu and Cu-Al alloys with systematic decrease in SFE. It was found that as SFE decrease from 78 mJ/m^2 of pure copper to 6 mJ/m^2in Cu-16%Al, grains size also reduces from 120 nm to 30 nm after ECAP processing

and simultaneously strength is significantly enhanced with increasing Al content or decreasing SFE [12].
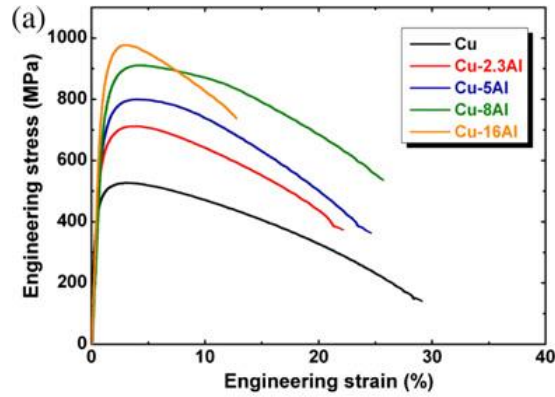
Fig.2.2.Typical engineering stress–strain tensile curves of the Cu and Cu– Al alloys[12]

In Cu-Zn and Cu-Al alloys there is lowering of SFE accompanied with the effect of solution hardening. Co and Ni elements have similar atomic diameter and their alloy experience very limited solution hardening. Thus, in order to isolate the effect of SFE on microstructure and mechanical properties Sun et al. studied Ni-Co alloys processed by HPT and rolling to study the effect of SFE on mechanical properties. It was shown that lowering of SFE decreases the grain size while simultaneously increases tensile ductility and strength[13].
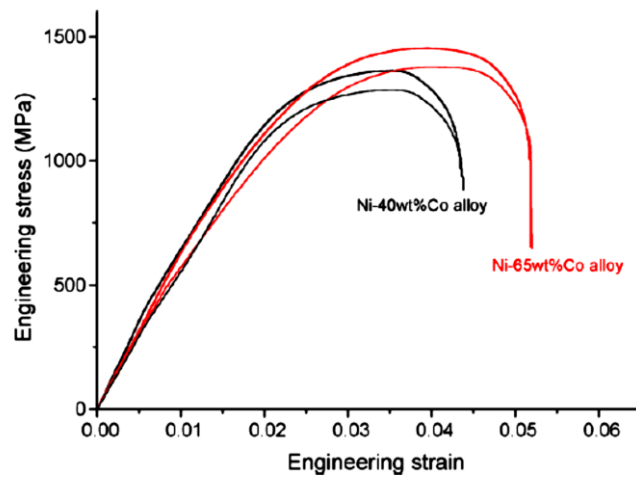
Fig.2.3.Engineering stress–strain curves for both Ni–40 wt.% Co alloy and Ni–65 wt.% Co alloy [13]

The brief but critical literature review shows that solution hardening due to alloying and reduction in stacking fault energy are closely interrelated and play major role on the evolution of microstructure, texture and mechanical properties. However, no systematic study has been carried out so far to isolate the effect of these parameters on the development of microstructure, texture and mechanical properties during SPD processing. The present research work makes an attempt to achieve this using Ni-Fe as a model system where alloying addition does not result in significant variation in SFE.

Chapter 3

Experimental procedure

3.1. Sample preparation for HPT processing:

For the present study various Ni-Fe alloys with compositions Ni-10%Fe, Ni-20%Fe and Ni-30%Fe were used. The starting materials were in the form of plates of thickness ~5mm. The thickness of these plates was reduced to 1 mm by multipass cold rolling. The cold rolled plates of the Ni-10%Fe, Ni-20%Fe and Ni-30%Fe were annealed for 1 hour at 500°C, 600°C and 600°C respectively. Samples for HPT processing in the form of 10 mm diameter disks were prepared from the annealed plates using wire cut Electrical Discharge Machine (Eazycut^{TM}, Electronica). The disks were further grinded using abrasive papers with grit size 1000 to 2000 to final thickness of 0.85 mm. Total eight disks of each alloy composition were prepared for subsequent HPT processing.

3.2. High Pressure Torsion Processing:

The processing by HPT was carried out at Research Center for Strategic Materials, National Institute for Materials Science, Japan. The HPT processing was conducted at room temperature using applied load of 390 KN which translates to imposed pressure of 5GPa and rotation speed of 1 rpm. The disks were processed to various strain levels, namely, N=1/12, 1/8,1/4, 1/2, 1,3,5 and 10 revolutions.

3.3.Characterization:

3.3.1.Microhardness measurements:

For microhardness measurement the HPT processed disks were mirror polished and measurements were taken across two perpendicular diameters at an incremental distance of 0.5mm using Vicker's indenter (EMCO-TEST™, Dura Scan-70) with applied load of 500 gm and dwell time of 15 seconds. The schematic illustration of microhardness test measurements is shown below in Fig.3.1.
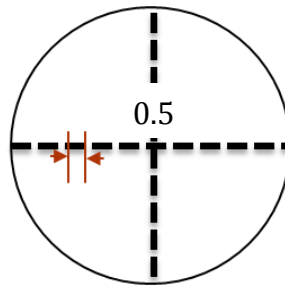

Fig. 3.1.Schematic illustration of microhardness test measurements

3.3.2 Microstructure and texture characterization:

One surface of each disk was polished to mirror finish and subsequently electropolished with a mixture of perchloric acid and ethanol (1:9 by volume). The microstructure and microtexture characterization were carried out by Electron Back Scattered Diffraction (EBSD) system attached to a FEG-SEM using Channel 5™ Software (Oxford Instruments, UK). EBSD measurements were taken on the top surface (r-ɵ plane) of disks at three different positions namely, center, mid radius and edge region of the disk as shown in the Fig.3.2. The measured data were used to

calculate the pole figure (PF) and Orientation distribution functions (ODFs). No sample symmetry was imposed i.e. triclinic sample symmetry was assumed.
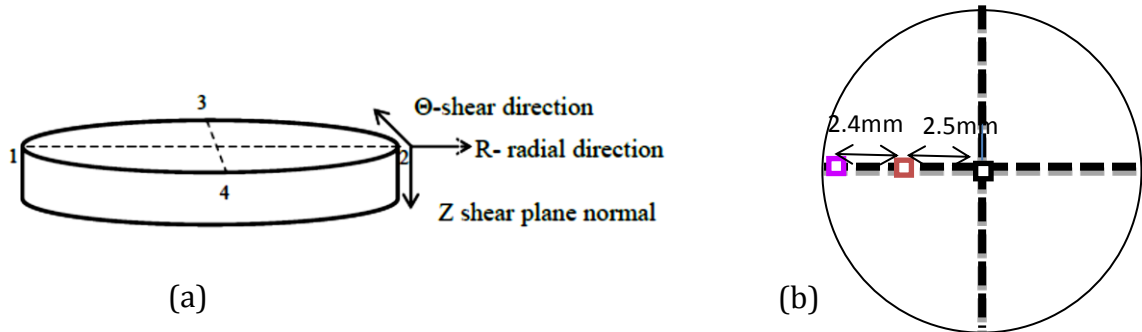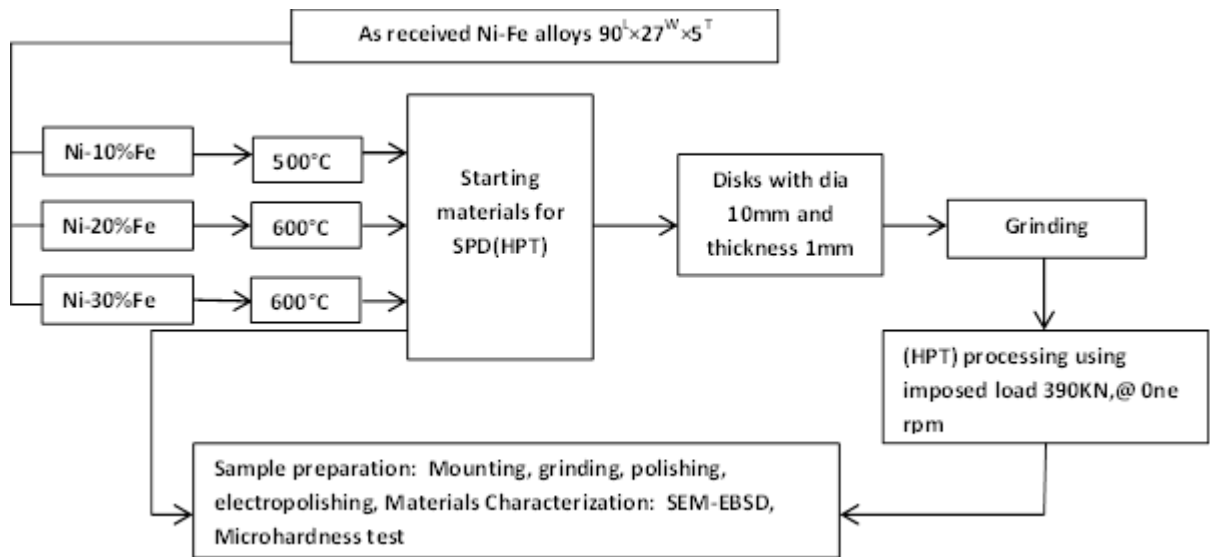

(a) (b)

Fig.3.2.(a)Sample geometry, (b)Schematic illustration of EBSD measurements

3.4 Flow chart of experimental procedure:

Chapter 4

Experimental Results

4.1.Starting materials characterization

4.1.1.X-Ray diffraction pattern of starting materials:Ni-Fe alloys

X-Ray diffraction was carried out on various Ni-Fe alloys. The XRD pattern shows that all Ni-Fe alloys used in the experiments form complete range of solid solution. The slight left shift in peaks indicates marginal increase in lattice parameter with increasing Fe content.
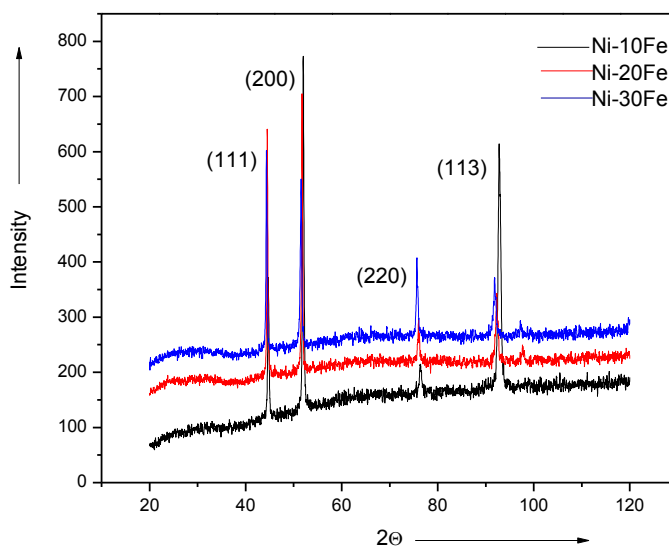

Fig.4.1.XRD pattern of starting materials for HPT disk-Ni-Fe alloys

4.1.2.Microstructure of the starting materials

The EBSD scans on the starting materials were obtained from the RD-TD plane. The grain boundary maps of Ni-10%Fe, Ni-20%Fe and Ni-30%Fe are shown in Fig.4.2. The Low angle grain boundaries (LAGB, 2°≤misorientation angle (θ)≤15°) and high angle grain boundaries (HAGB, θ> 15°) are shown by red and black lines, respectively. The average grain size calculated by the line intercept method is 8μm, 7μm and 5μm respectively for Ni-10%Fe, Ni-20%Fe and Ni-30%Fe. In Ni-10%Fe some large grains are also observed.

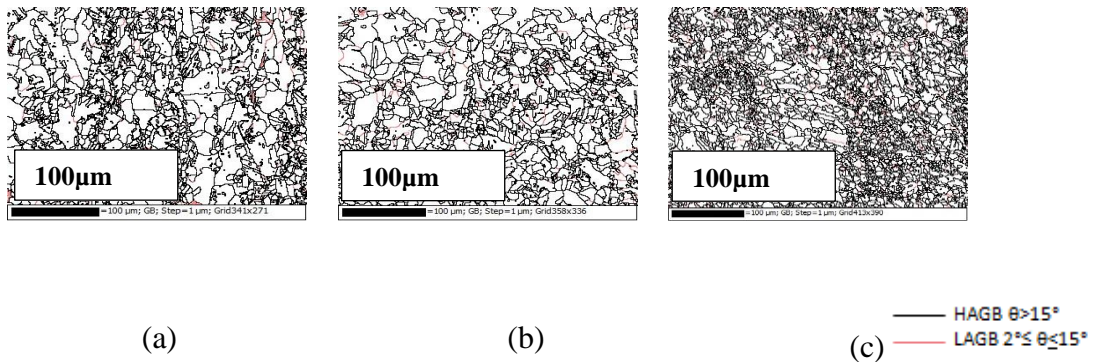(a)   (b)   (c)

Fig.4.2.GB Maps of starting material (a) Ni-10%Fe, (b) Ni-20%Fe and

(c) Ni-30%Fe

4.1.3 Microhardness measurements of starting material

The results obtained from the Vickers microhardness test of the starting materials are shown in Fig.4.3. The average microhardness of starting material was calculated by taking measurements at 15 different points with applied load of 500 gm and dwell time of 15 sec. The average microhardness of Ni-10%Fe, Ni-20%Fe and Ni-30%Fe was found to be 142,159 and 172 respectively. The microhardness value of the starting materialsis found to increase with increasing Fe content.
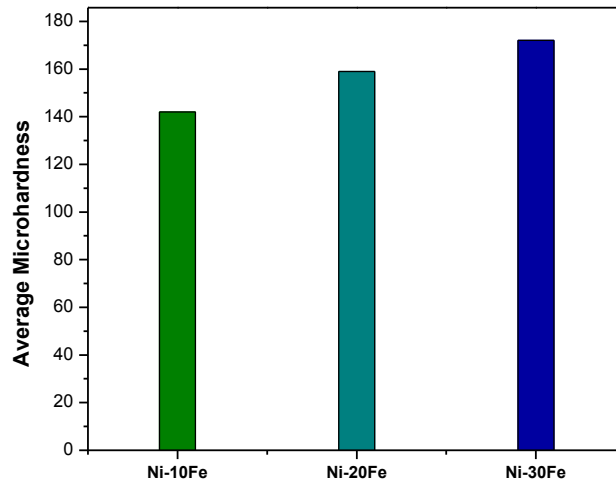
Fig.4.3.Average microhardness of starting material

4.2.Microstructure evolution in HPT Processed Ni-Fe alloy

4.2.1 Microstructure Characterization of HPT Processed Ni-10%Fe

Figure4.4 shows the microstructure evolution with increasing number of rotations at three radial positions (center, mid-radius and edge) on the disk plane. For Ni-10%Fe alloy, the average grain size decreases drastically from 8.4 µm in center region to 390nm and 270 nm in middle and edge regions, respectively after N=1/2 rotation. This results in the increase of HAGB from ~8% in center region to ~46% and ~75% in middle and edge regions, respectively. This indicates pronounced inhomogeneity in the processed disks. Even after N=1 rotation the grain size at the center region is rather large ~855 nm and fraction of HAGB is low ~0.35. The homogeneity of the disks increases substantially following N=5 rotations so that the fraction of HAGB is found to be almost similar (~77%) at different radial locations.

The grain size in middle and edge regions after N=10 rotations is slightly larger than those observed after N=5 rotations. At the middle, the grain size increases from 155 nm after N=5 rotations to 177 nm after N=10 rotations while for the edge region the grain size increases from 175 nm after N=5 rotations to 185 nm after N=10 rotations. The variation in grain size and HAGB fraction with strain at different radial locations in Ni-10%Fe alloy is summarized in Fig.4.5.
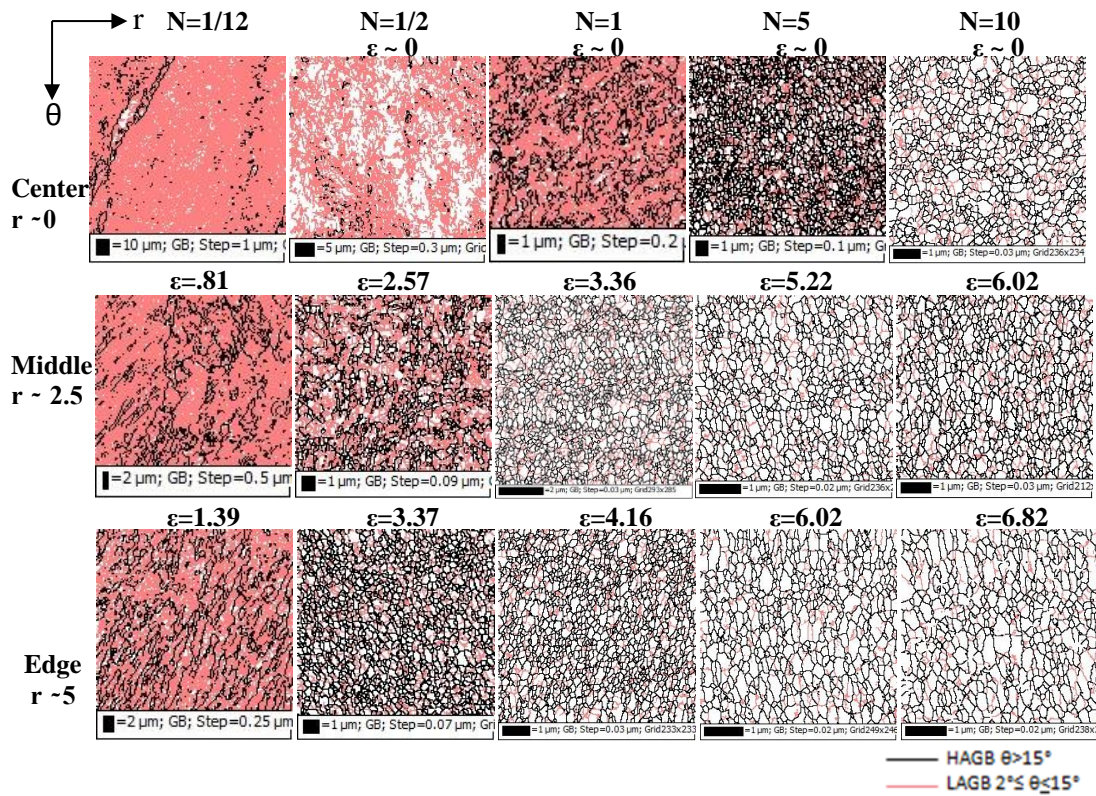

Fig 4.4.Grain boundary maps of HPT processed Ni-10%Fe alloy at center (r ~ 0), middle (r ~ 2.5) and edge (r ~5 mm) regions obtained after different numbers of rotations (N) 1/12,1/2,1,5 and 10.

(a)

(b)

Fig.4.5.Variation of (a) grain size (b) HAGB fraction with strain at different

radial locations in Ni-10Fe alloy.

4.2.2. Microstructure Characterization of HPT Processed Ni-20%Fe

The grain boundary (GB) maps of Ni-20%Fe are shown in Fig.4.6. At lower strains (N=1/12) the grains are rather coarse and fraction of LAGBs is high across

the disk. At N=1/2 inhomogeneity in the microstructure in the central region is evidenced by the presence of both large and much smaller grains. At N=1 grain size reduces significantly from 1.53 μm in the center region to 181 nm at the middle region with concomitant increase in the HAGB from 22% at the center region to 65% at the middle region. The grains in the center of disk also appear slightly elongated. After N=5 rotations, large grains (~400 nm) and high fraction of LAGBs is confined only in central region. With increasing number of turns homogeneity is achieved in the microstructure. This is evident from microstructure obtained after N=10 rotations characterized by equiaxed grains of size ~168 nm with fraction of HAGBs ~78%. The variation in grain size and HAGB fraction at different radial locations in Ni-20%Fe is summarized in Fig.4.7.

Fig.4.6.Grain boundary maps of HPT processed Ni-20%Fe alloy at center (r ~ 0), middle (r ~ 2.5) and edge (r ~5 mm) regions obtained after different numbers of rotations (N) 1/12,1/2,1,5 and 10.
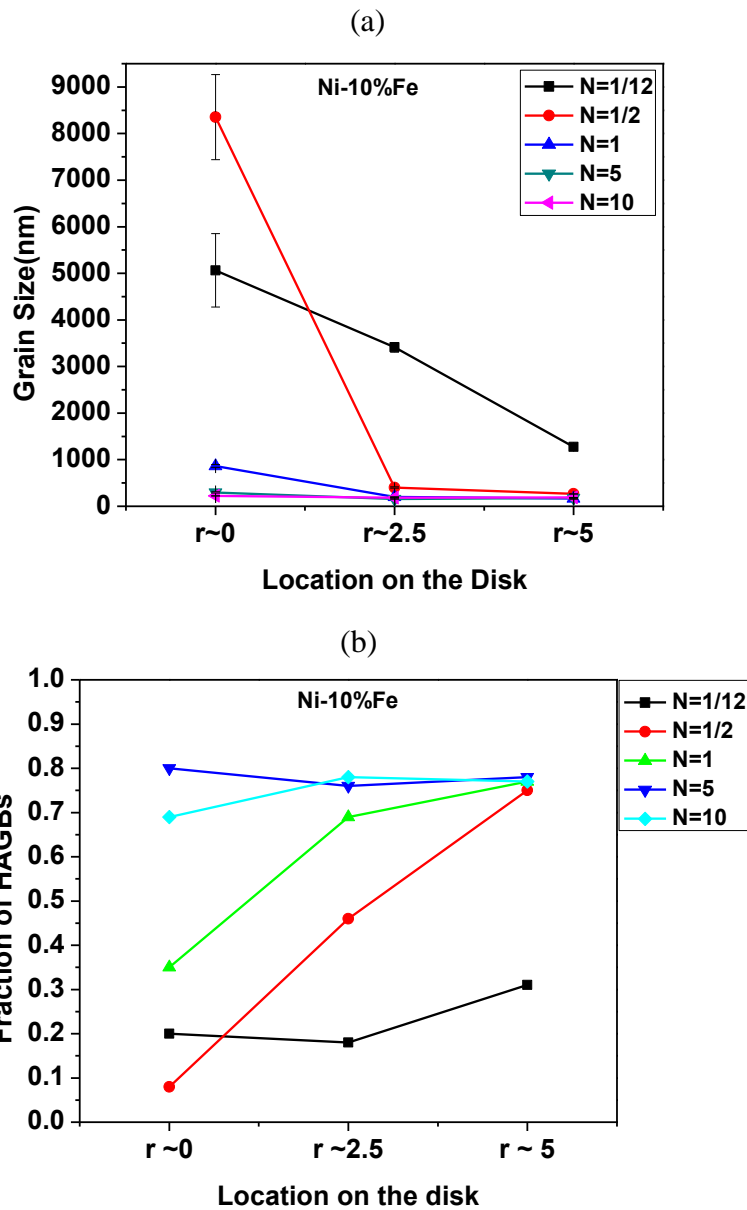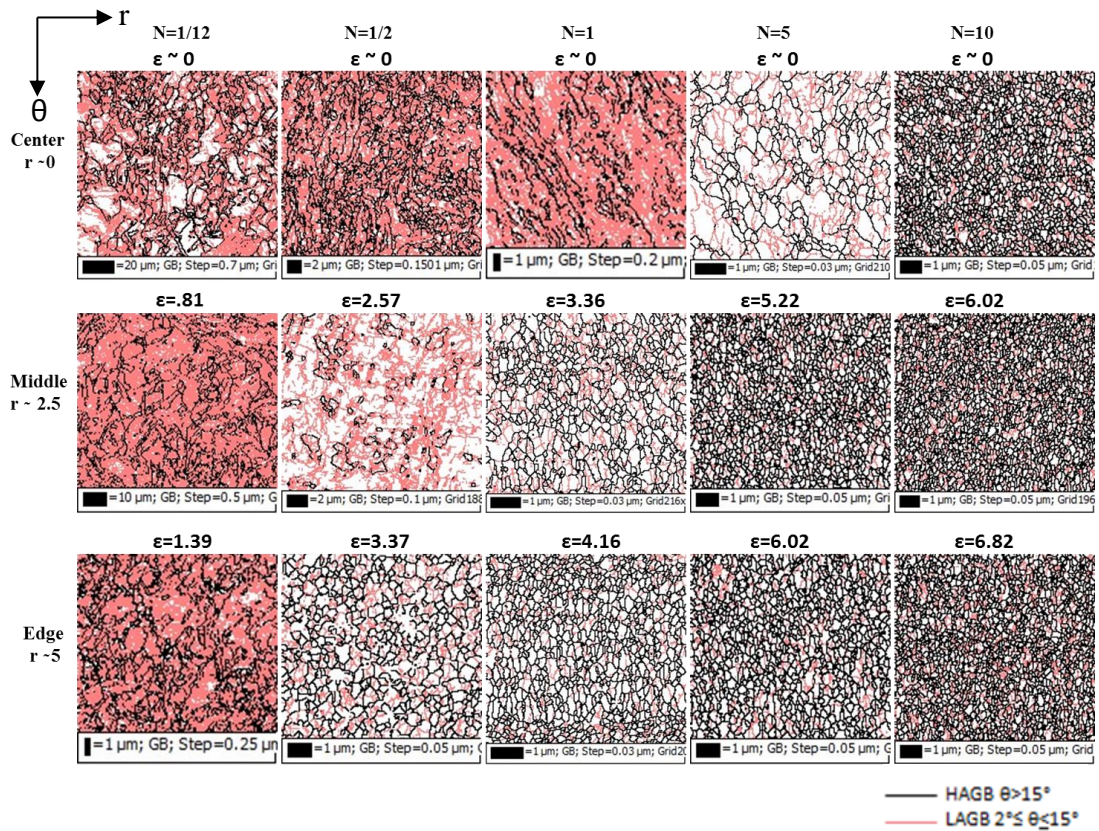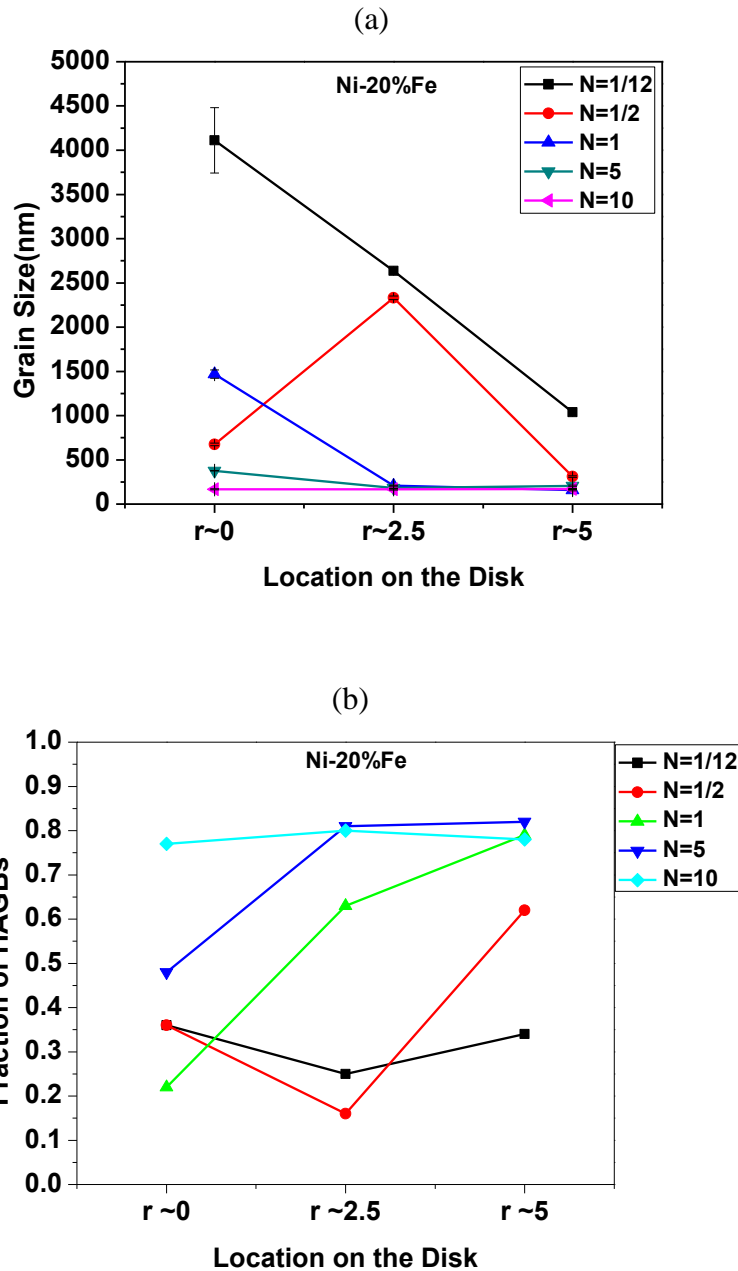
(a)

(b)

Fig.4.7.Variation of (a) grain size, (b) HAGB fraction with strain at different radial locations in Ni-10%Fe alloy.

4.2.3 Microstructure Characterization of HPT Processed Ni-30%Fe

Figure.4.8 shows the GB maps of Ni-30%Fe at different strain levels obtained from different radial locations on the disk plane. It can be seen from the GB maps that after N=1/12 rotations, the grains are rather large with high fraction of LAGBs (~27%) across the disk. After N=1/2 rotations, the center region of the disk have fragmented grains, but in middle region the microstructure shows mix of very coarse and small, fragmented grains. After N=1 rotation, the fraction of HAGBs increases drastically from ~35% at the center region to ~75% at the edge. This is accompanied by sharp reduction in even grain size from ~1um in the center region to 165 nm at the middle. The grain size decreases continuously with concomitant increase in the HAGB fraction at the center region with increasing number of rotations. However, at the middle and edge regions slight increase in grain size is observed with increase in strain beyond N=5 rotations. The variation in grain size and HAGB fraction at different radial locations in Ni-30%Fe is summarized in Fig.4.9.
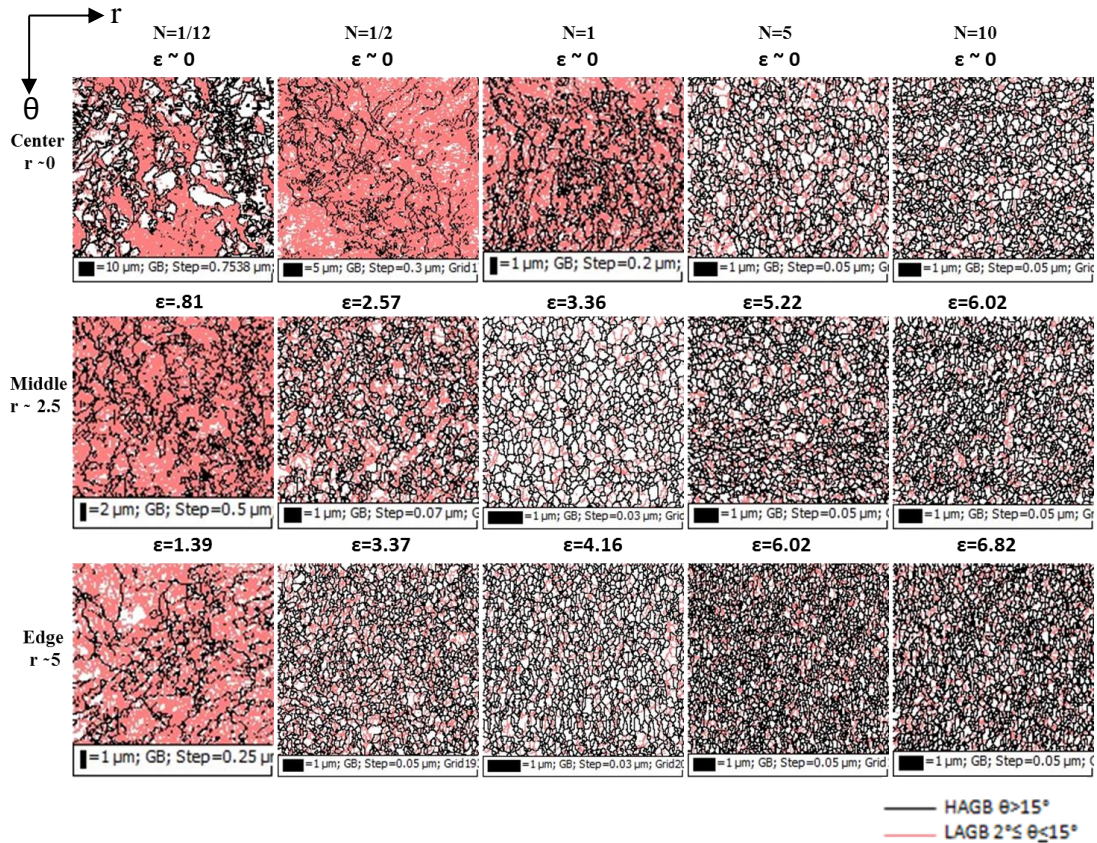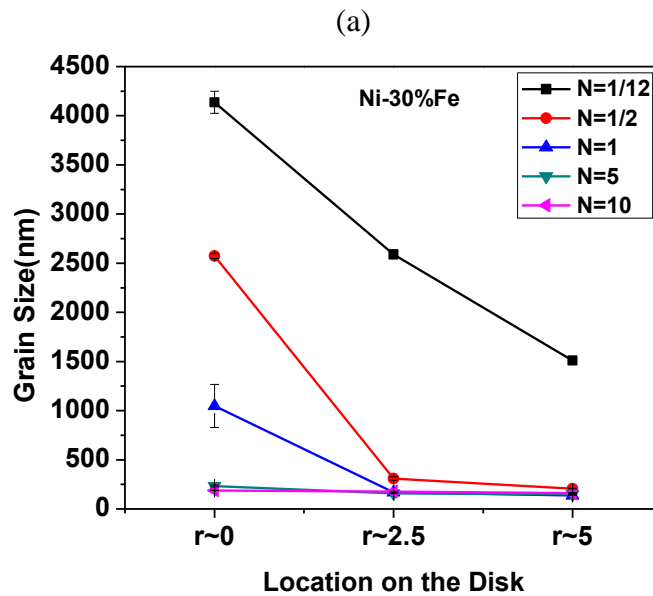
Fig.4.8.Grain boundary maps of HPT processed Ni-30%Fe alloy at center (r ~ 0), middle (r ~ 2.5) and edge (r ~5 mm) regions obtained after different numbers of rotations (N) 1/12,1/2,1,5 and 10.

(a)

(b)
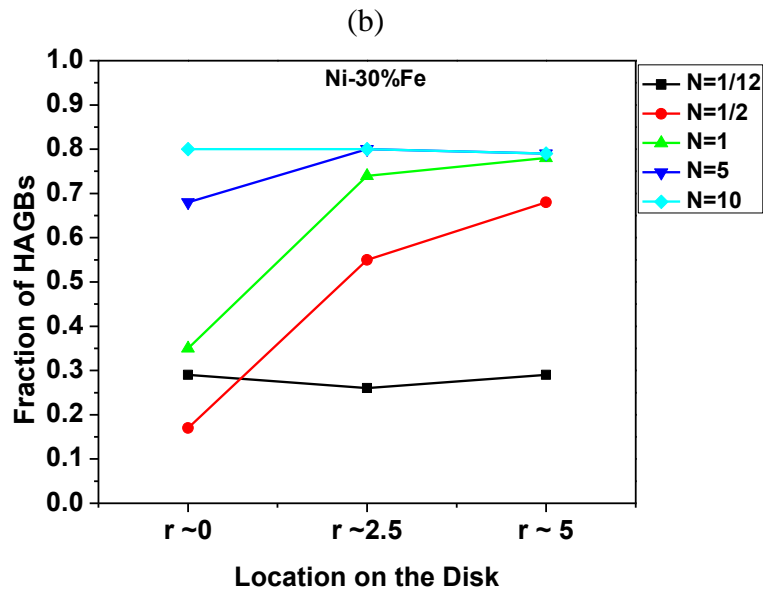
Fig 4.9. Variation of (a) grain size (b) HAGB fraction with strain at different radial locations in Ni-10Fe alloy.

4.3. Microtexture evolution in HPT Processed Ni-Fe alloys

HPT processing occurs by simple shear . Shear texture is generally described in terms of two fiber, A fiber ({111}<uvw>) and B fiber ({hkl}<110>), where {hkl} is plane parallel to shear plane(r-θ) and <uvw> is parallel to shear direction[14]. The ideal crystallographic orientations for simple shear in FCC metals are shown in Table 4.1.

Table 4.1.Ideal orientations of FCC metals under simple shear [14]

Shear Components	Miller Indices{hkl}<uvw>
A	{1-1-1}<110>
A-	{-111}<-1-10>
B	{-112}<110>
B-	{1-1-2}<-1-10>
C	{001}<110>
A1*	{-1-11}<112>
A2*	{11-1}<112>
{111}fiber	{111}<uvw>
<110>fiber	{hkl}<110>

Figure 4.10 shows the (111) pole figures obtained from the edge regions at various rotations. At small strains (N=1/12) the intensities are strong around A1*/A2* and C components in Ni-10%Fe (Fig. 4.10a). However, in Ni-20%Fe and Ni-30%Fe these intensities decrease (Fig. 4.10f and 4.10k). In all pole figures after 1/2 rotation intensity are low (not more than 2.5 times random). After 5 rotations there is no significant difference in the pole figures of Ni-10%Fe, Ni-20%Fe and Ni-30%Fe apart from the fact that for N=1 to N=10 rotations intensities around B/B-component are absent in Ni-10%Fe (Fig.4.10c-e) but could be observed in Ni-20%Fe (Fig.4.10h-j) and Ni-30%Fe (Fig.4.10m-o).
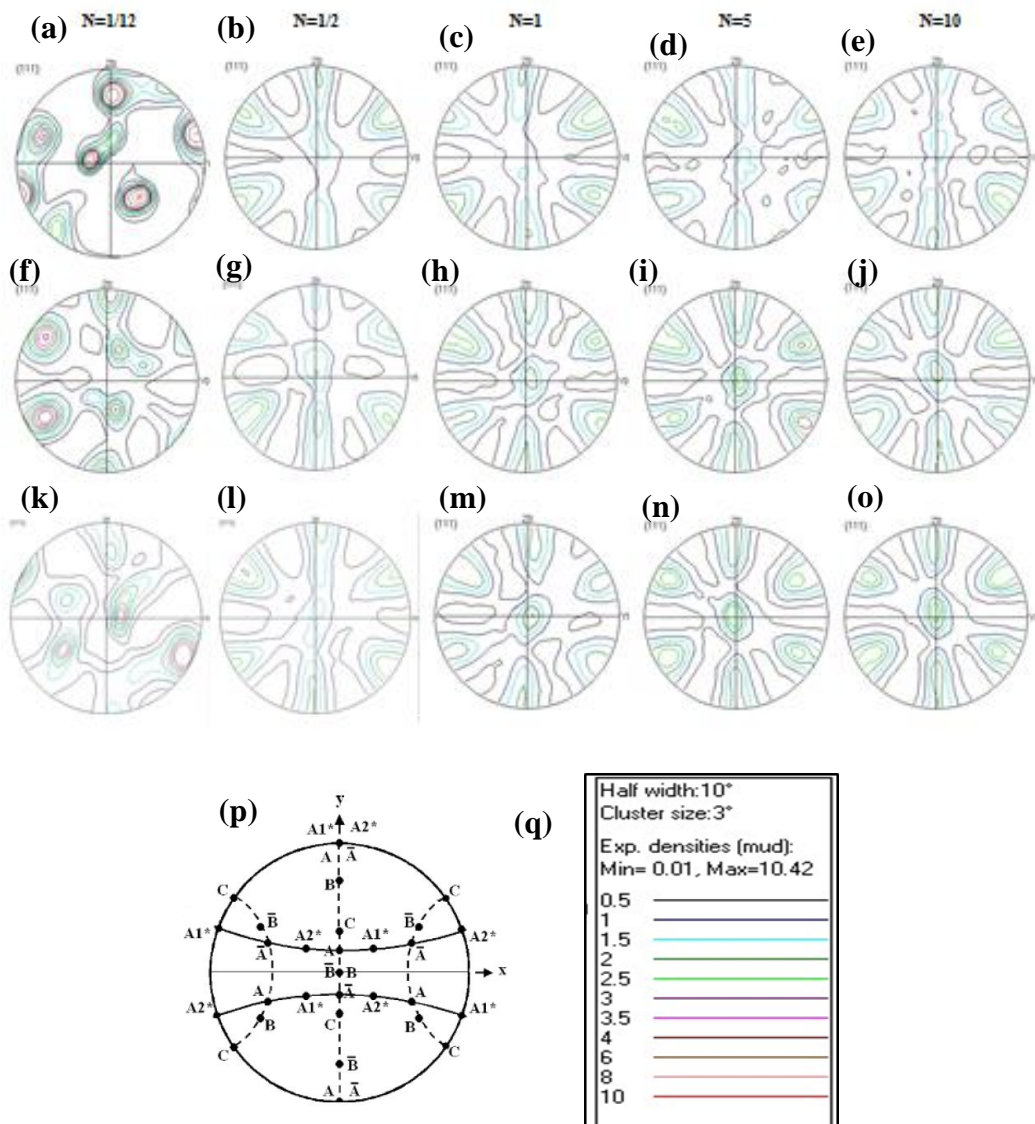
Fig 4.10.(111) Pole Figures at r~5 (edge regions) in HPT processed, Ni-10%Fe (a-e), Ni-20%Fe(f-j) and Ni-30%Fe (k-o) at N=1/12, 1/2, 1, 5 and 10, (p)Ideal shear orientation in (111) pole figure and (q)Texture intensity legends

In order to further understand the differences in texture of the three alloys, orientation distribution functions (ODF) were calculated using the harmonic series expansion with a series rank of 22 (lmax=22) and Gaussian smoothing of 5°. Figure

4.11 shows the plots of Φ2=45° sections of the ODF of the edge regions of the HPT disks of different rotations. In Ni-10%Fe at N=1/12 rotations, some intensities around B ({hkl}<110>) fiber are observed (as represented in Fig 11.a). After N=1/2 turns, A fiber is present at all strain values but it becomes discontinuous as the number of turns increases. C component is also observed with low intensities in almost all strain values (Fig.11(a)-11(e)). In Ni-20%Fe A fiber is observed at all strain values except for N=1/2. There is a strong presence of B component at N=1/2, which is also consistent with texture component fraction (~17%). After one rotation, a component very close to {112}<11-1> shows strong intensities at all strain values(Fig 11(f)-11(j)). In Ni-30%Fe there is weak presence of C component at almost all rotations. A fiber is present at all strain level but it becomes discontinuous at higher strain levels. After N=1/2 turns, {112}<11-1> component becomes stronger as the number of turns increases (fig.11(l)-11(o)). There is not much difference observed in Ni20%Fe and Ni-30%Fe after one rotation.
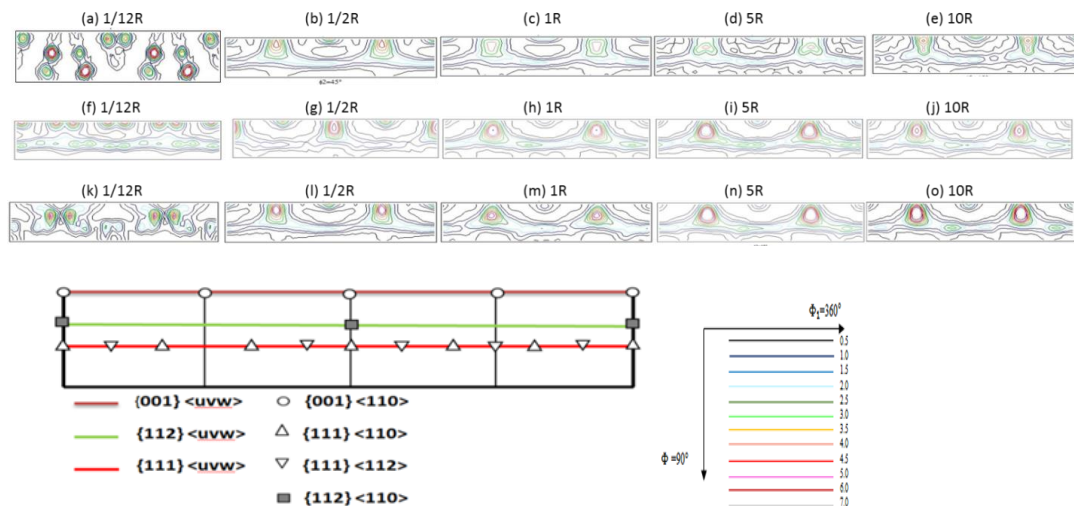

Fig 4.11.φ2=450 ODF section of HPT processed Ni10%Fe (a-e), Ni-20%Fe (f-j)and Ni30% Fe (k-o)at edge region; position of ideal shear texture below[15]

The grain orientation maps (GO map) at the edge regions of Ni-10%Fe, Ni-20%Fe and Ni-30%Fe at various rotations are shown in Fig.4.12.Figure 4.13summarizes the variation of volume fraction of different texture components at various strains only at the edge regions of the disks for the three Ni-Fe alloys. Note, that only the edge regions are shown here for comparison purpose as the highest strain is obtained at this region such that greatest change in texture is expected for this region only.

In all three Ni-Fe alloys A/A- , A1*/A2* and C are the major shear orientations at all strain values. Other than ideal shear components, {112}<11-1> component is quite strong in all the Ni-Fe alloys at different strain levels. Volume fraction of {112}<11-1> component increases with increasing Fe content. In Ni-10%Fe volume fraction of the A/A- remains largely unchanged (~8%) with increasing strain. Volume fraction of the A1*/A2* and {112}<11-1> component increases sharply after N=1/12, thereafter it remain almost stable with further increase in strain. Volume fraction of C component increases as strain increases. There is a weak presence of B component of ~ 2% at all rotations.

In Ni-20%Fe weakening of all the shear components is witnessed with increasing strain. Strong presence of the A/A- and A1*/A2* (~11%) is revealed, particularly, at lower strain (ε~1.39). However, the {112}<11-1> component is strengthened with increasing strain. The B/B- component has strongest presence after N=1/2 rotations (~16%) but does not reveal substantial presence at other strain values (~2%).
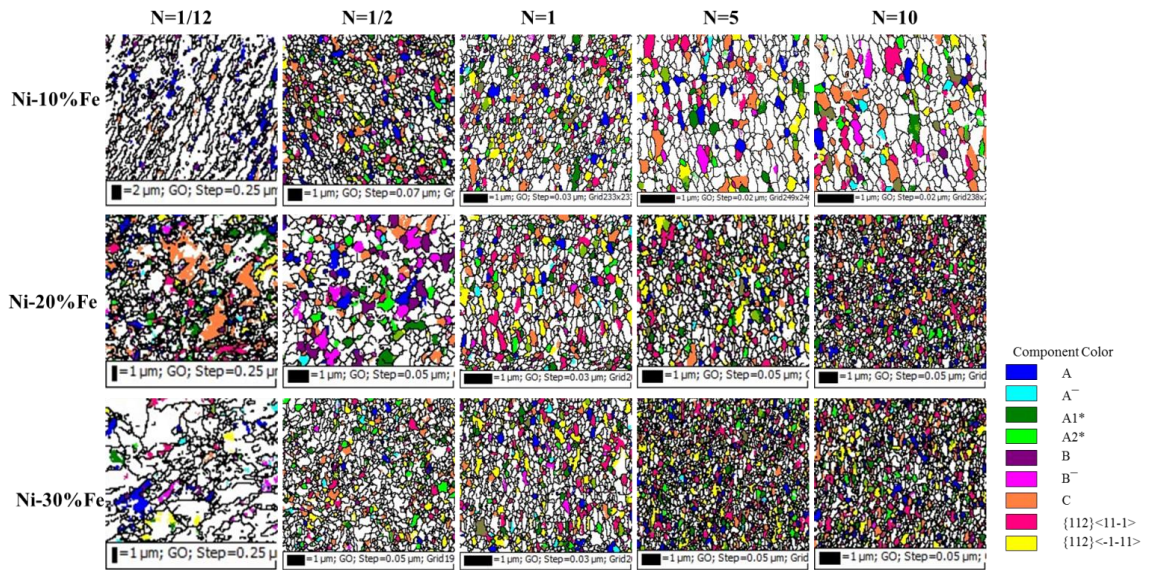
Fig.4.12.Grain orientation maps of Ni-Fe alloys at edge regions (r~5mm) for different numbers of rotation(N) 1/12, 1/2 1,5, and 10.

In Ni-30%Fe also, there is a small drop in volume fractions of all texture components as number of turns increases except for A1*/A2* and {112}<11-1>which increases with increasing rotations. The C component increases sharply from ~0.5% at N=1/12 rotation to ~8.5% at N=1/2 rotation. At N=10 volume fraction of all texture component decreases as alloying increases except for A1*/A2* which increases slightly and there is significant increase in volume fraction of {112}<11-1> component.

(a)
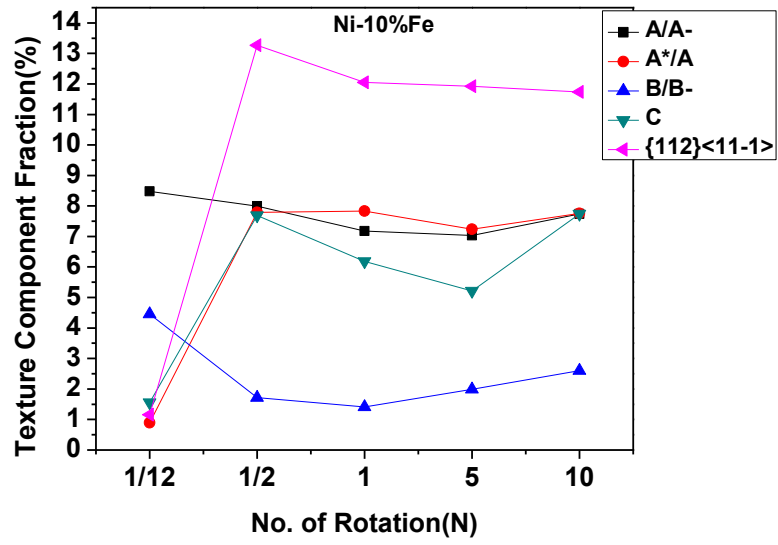
(b)
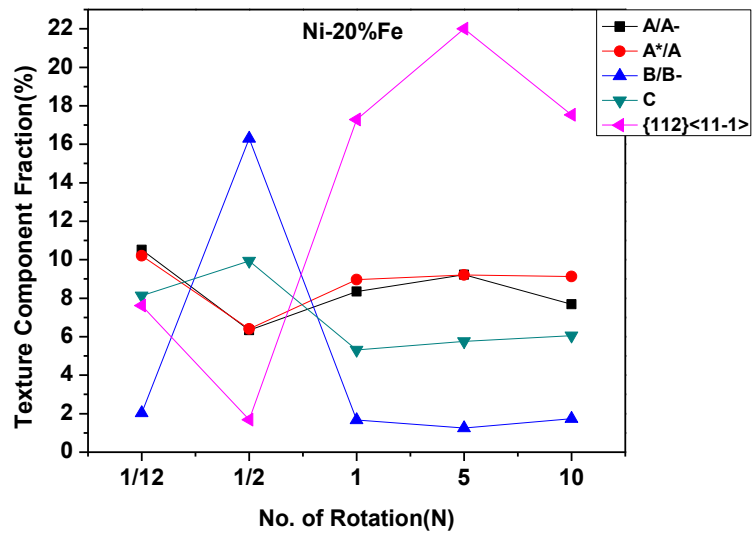
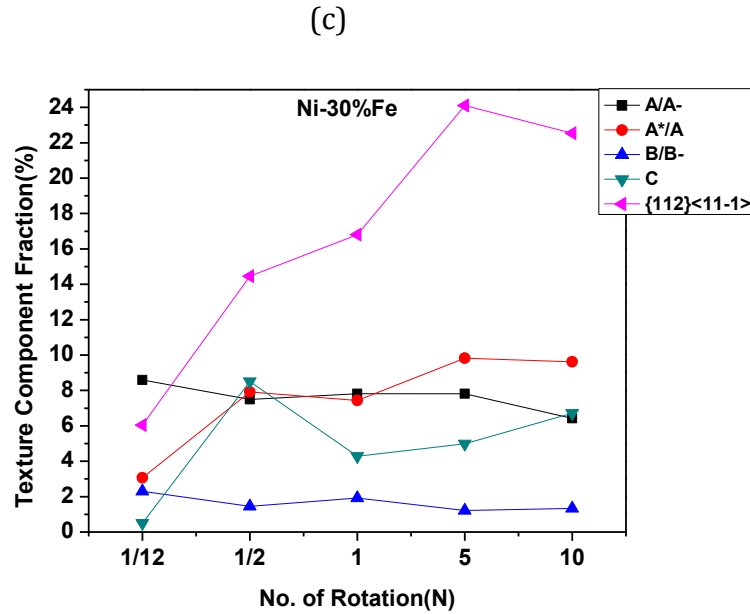**Fig 4.13.Volume fraction of ideal shear texture components at edge regions for different numbers of rotations (N)in Ni-Fe alloys: (a) Ni-10%Fe, (b) Ni-20%Fe and (c) Ni-30%Fe**

4.4.Microhardness measurements of Ni-Fe disks after HPT

The microhardness of HPT processed disks (Fig.4.14) was taken along the diameter of the disks at incremental distance of 0.5 mm using applied load of 500 gm and dwell time of 15 sec. Hardness values show gradually increase from the center to the edge with increasing number of rotations. The microhardness profile from the center to the edge in Ni-20%Fe and Ni-30%Fe is quite similar and considerable inhomogeneity in microhardness is observed between the center and edge regions even up to the highest strain level. However, in Ni-30%Fe homogeneity is achieved across the disk after 10 rotations. The microhardness values of Ni-10%Fe, Ni-20%Fe and Ni-30%Fe at the edge region are ~418Hv,~465Hv and ~472 Hv, respectively after 10 rotations.
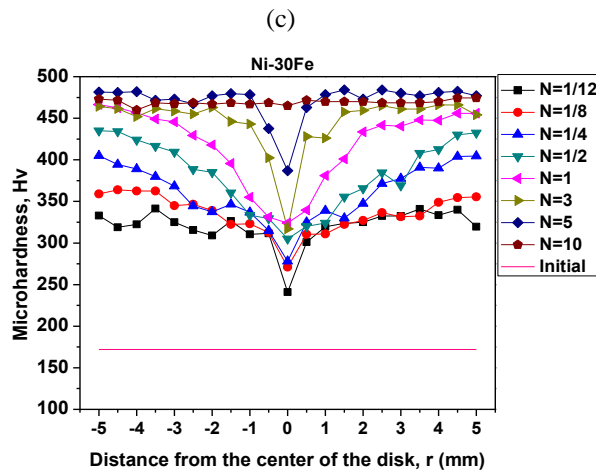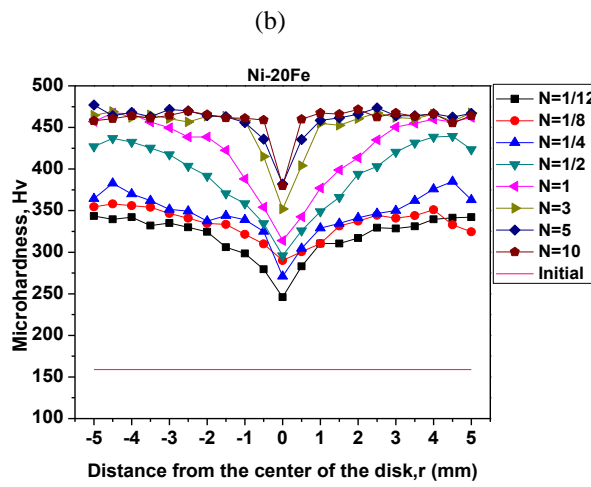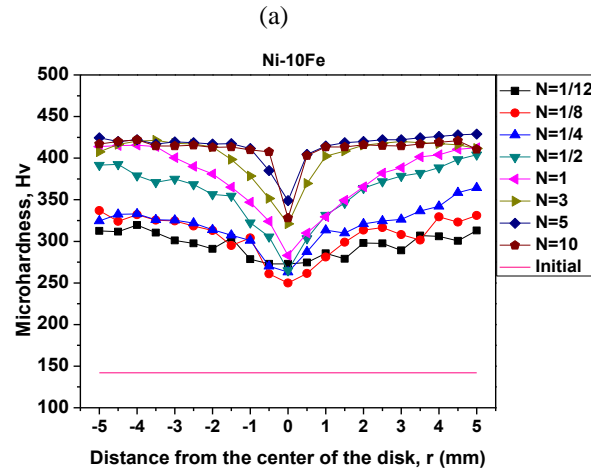
(a)

(b)

(c)

Fig 4.14.Hardness evolution plot in (a) Ni-10%Fe (b) Ni-20%Fe (c) Ni-30%Fe

Chapter 5

Discussion

5.1. Microstructural evolution and hardness of HPT processed alloys

In the present study various Ni-Fe alloys (Ni-10%Fe, Ni-20%Fe and Ni-30%Fe) have been deformed by HPT to various strain levels using an applied load of ~5 GPa. The variation in microstructure from center to the edge region can be clearly seen in Fig.4.4, Fig.4.6 and Fig.4.8. This variation in microstructure is due to the varying strain values across the disk. However, at N=10, homogenous microstructure can be seen across the disk in Ni-20%Fe and Ni-30%Fe. It has been proposed that shear starts at the region where friction coefficient is the greatest. This induces local hardening due to which there is a reduction in frictional force and shearing is transferred to another point [2]. In all the three alloys it is observed that at lower strain values coarser microstructure exists with a high fraction of LAGBs. With increase in the imposed strain the microstructure is refined and fraction of HAGBs is also increased.

Evolution of microstructure in HPT demonstrates the same behavior as observed in other deformation routes [16]. Considering microstructural evolution in detail it follows that grain subdivision is the main mechanism for microstructural refinement [16, 17]. Grains are subdivided into cell block structure on a finer and finer scale. In metals and alloys having high to medium stacking fault energy dislocations can move easily by cross slip. The mobility of dislocations leads to the formation of

32

dislocation boundaries and grain boundaries, sub-dividing the deformation microstructure. At low strains there are cellular subgrains which transforms to grains with HAGB at higher strains. With increasing strain misorientation angle increases and so the fraction of HAGB[16].

As number of rotations increases grain size decreases, however, in all the three alloys grain size is minimum after one rotation. Thereafter, there is a slight increase in the grain size as can be seen in Table 5.1. Remarkable homogeneity of microstructure is achieved in both Ni-20%Fe and Ni-30%Fe alloys after N =10 rotations (Fig 4.7a and Fig 4.9a). Figure 5.1 shows the fraction of HAGB and grain size plots of the three alloys at N=10. It can be observed that the behavior of Ni-20%Fe and Ni-30%Fe are almost similar, so that, the HAGB fraction and grain size is uniform across the disk.
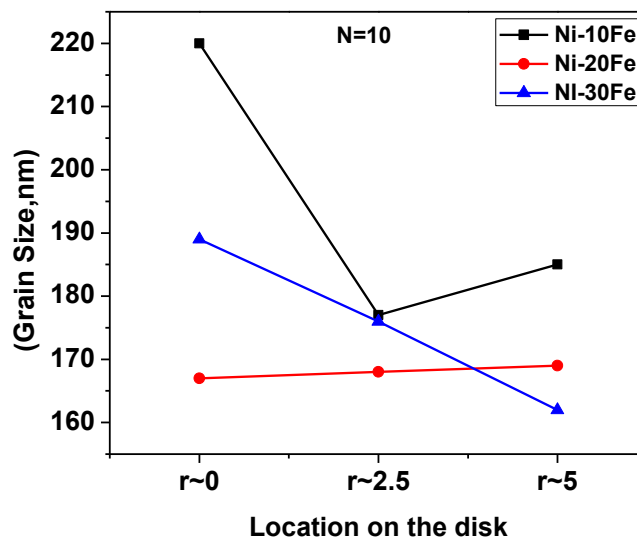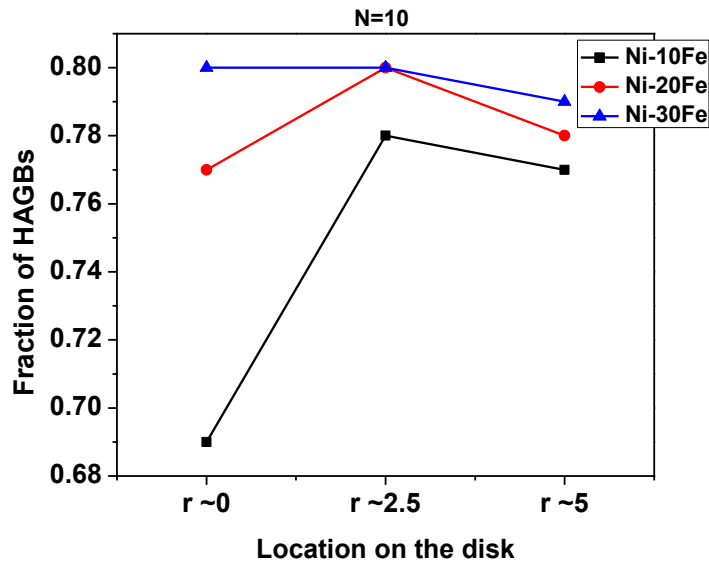
Fig 5.1.Grain size and HAGB fraction at the center, middle and edge regions of Ni-10%Fe, Ni-20%Fe and Ni-30%Fe at N=10 disks.

Figure 5.2 shows a plot comparing the grain sizes of the edge region (highest strained region) of the disk of all the three alloys at various rotations. Reduction in grain size with increasing solute concentration can be observed, except for N=1/12 which corresponds to a very low strain value so that the formation of deformation induced grains is not complete and only fragmented structure with large fraction of LAGB can be observed.

Fig 5.2.Grain size of Ni-10%Fe, Ni-20%Fe and Ni-30%Fe at the edge regions at various deformation levels.

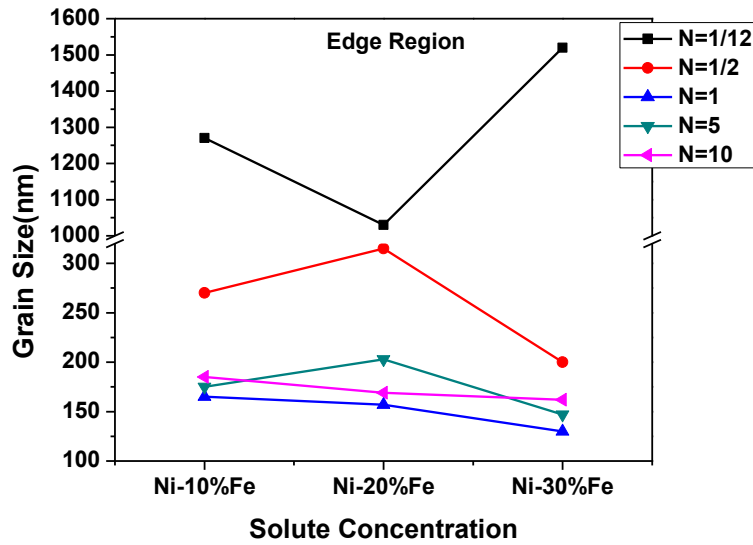In Ni-Fe alloys SFE is not significantly affected by alloying [7]. Thus, the grain refinement is primarily affected by solute hardening. The shear strain required for dislocation motion increases in the presence of solute atoms via several interactions , namely, elastic interaction (difference in atomic size of solute and matrix), modulus interaction (shear modulus mismatch), electrical interaction (change in valence electron per atom) and chemical interaction (difference in stacking fault energy) [18]. It has been documented in literature [18] that amongst these interactions elastic and modulus interaction is more dominant factors contributing to solution hardening. Steady state grain size is achieved during SPD when accumulation of dislocation balances dislocation annihilation and grain boundary movement. Solute atoms increases the stress required for dislocation motion and thus promotes

dislocation accumulation. Due to this the steady state grain size should be reduced by alloying [18].

For better understanding of the factors affecting grain refinement, we compare two alloy systems, namely, Ni-Fe and Ni-Co [19]. While in the Ni-Fe alloy system change in SFE is negligible as already stated, in Ni-Co system the SFE is systematically decreased with increasing alloying without significant solution hardening[7]. Comparing the two alloy systems it can be seen that there is not much difference in the microstructural parameters, for e.g. grain size, fraction of HAGB and misorientation angle at the edge regions.

It may be observed that, although, the microstructural parameters are comparable in both the alloy series, the formation mechanism may be different. In Ni-Fe alloys the minimum in grain size is achieved much earlier (i.e. after N=1 rotation) as compared to the Ni-Co alloy series. Ni-30%Fe evidently shows lower grain size as compared to the two other Ni-Fe alloys after N=1 rotation. However, the difference in grain size is not as significant as in the Ni-Co alloy series. If the alloying effect in two alloy systems is considered, it can be noticed that with increasing alloying content from 20%Co to 60%Co the grain size is drastically reduced in Ni-Co system after N=10 rotations indicating that additional grain refinement is operative in low SFE alloys, such as, Ni-60%Co.

It may be noticed that in low SFE alloys the mechanism of grain refinement proposed involves formation of deformation twins. The accumulation of dislocations can convert deformation twin boundaries (TBs) into random HAGBs resulting in addition structural refinement [20]. This could explain the smaller grain size in Ni-

60%Co alloys with the least SFE amongst the three Ni-Co alloys. Therefore, when the contribution of solution-hardening is not significant the SFE plays a significant role in obtaining minimum ultrafine grain size. This variation in grain size can also be observed in Table 5.1 which shows that the grain size of Ni-Fe and Ni-Co alloys in the edge region at various strain levels. It can be observed that the structural evolution is faster in Ni-Fe alloy series. The final grain size achieved after N=10 rotations in Ni-30%Fe and Ni-60%Co is almost identical indicating that solute-hardening is also as effective in obtaining ultrafine grain size. This also agrees well with the recently published results where it is reported that there is no distinct trend observed in various alloys having different SFE (Fig 5.4). Irrespective of the SFE the steady state grain size is similar which indicates that SFE is not the only dominating parameter responsible for grain refinement [18]. However, the interesting point is that in all the alloys where there is evident structural coarsening at different stages of deformation only the Ni-60%Co shows consistent decrease in grain size down to N=10 rotations. While it may be ascribed to the additional grain refinement in low SFE via the mechanism already discussed, the role of low SFE in restricting the motion of partial dislocations should also be emphasized. Even though the solute hardening is effective in achieving similar ultrafine grain size as demonstrated in Ni-Fe alloy series, structural coarsening is evident as SFE is not lowered by alloying.

It can thus be concluded that structural evolution is faster during severe plastic deformation in alloy systems where alloying results in solute-hardening. In alloy systems where the solute-hardening is minimum, structural evolution is slower and lowering of SFE is crucial in achieving the minimum ultrafine grain size. The major

contribution to this end arises from the mechanism involving formation of deformation twins and resistance to structural coarsening.
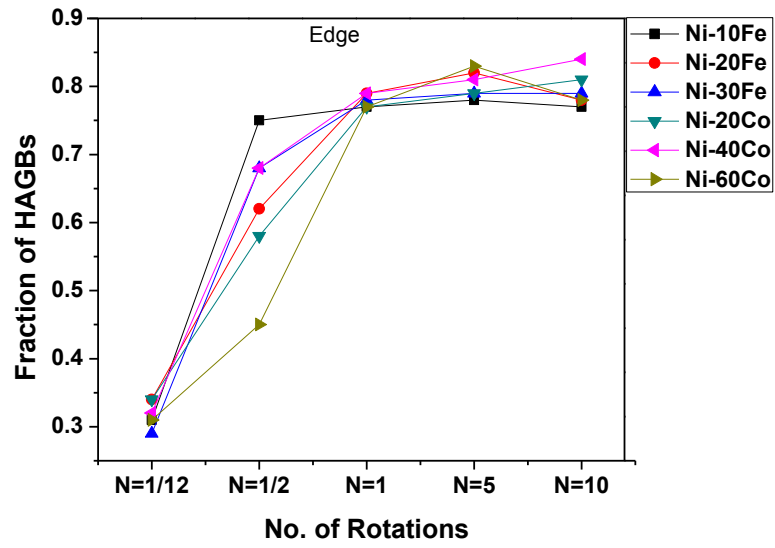
Table 5.1.Grain Size of Ni-Fe and Ni-Co alloys at different rotations at edge region

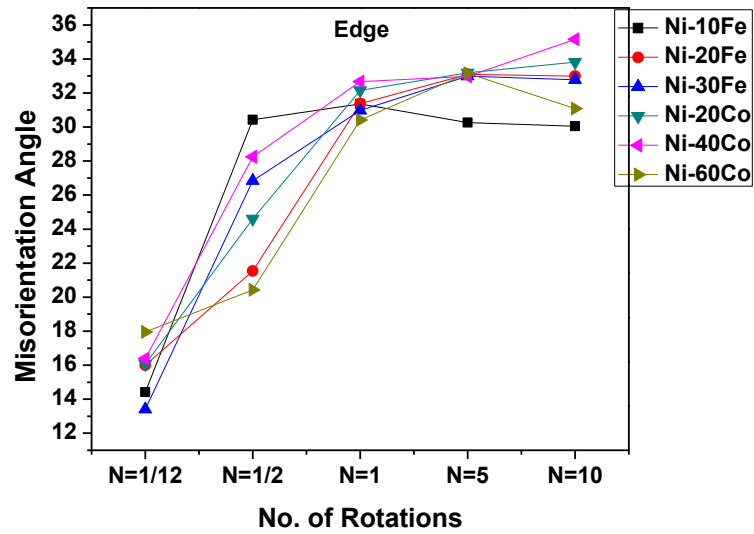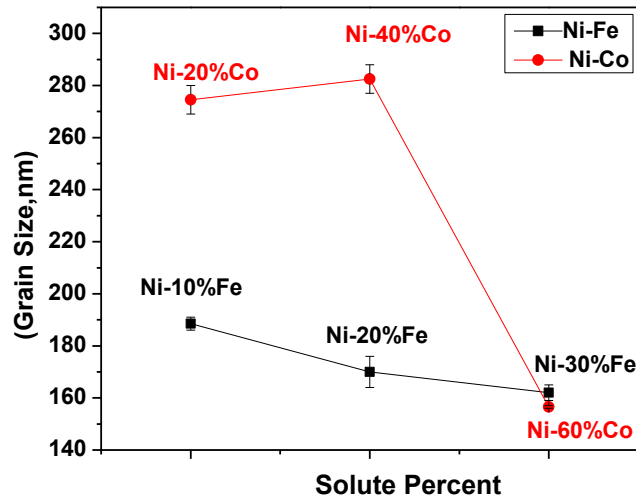| No. of Rotations(N)	Ni-10%Fe (nm)	Ni-20%Fe (nm)	Ni-30%Fe (nm)	Ni-20%Co (nm)	Ni-40%Co (nm)	Ni-60%Co (nm)
(Starting material)	8230	6630	4540	7870	5320	4710
1/12	1270	1030	1520	840	795	805
1/ 2	270	315	200	319	335	385
1	165	157	130	225	160	185
5	175	203	147	200	195	165
10	185	169	162	270	295	155

(a)
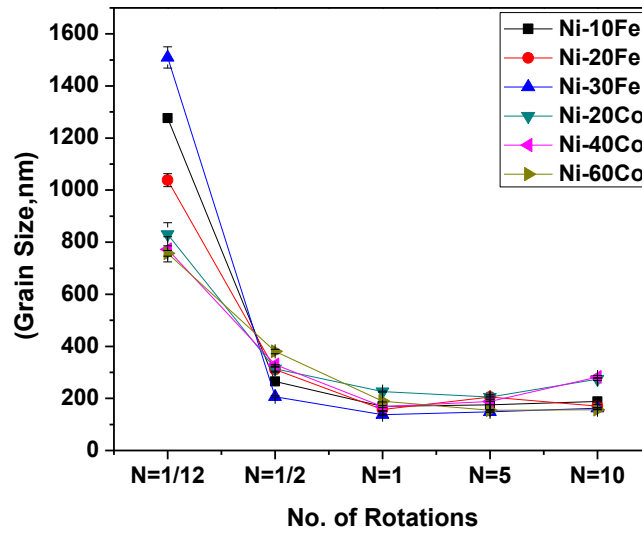
(b)

(c)

(d)

Fig.5.3.Variation in (a) Grain size (b) Fraction of HAGB, (c) Misorientation angle at various no. of rotations and (d) Variation in grain size with alloying content.
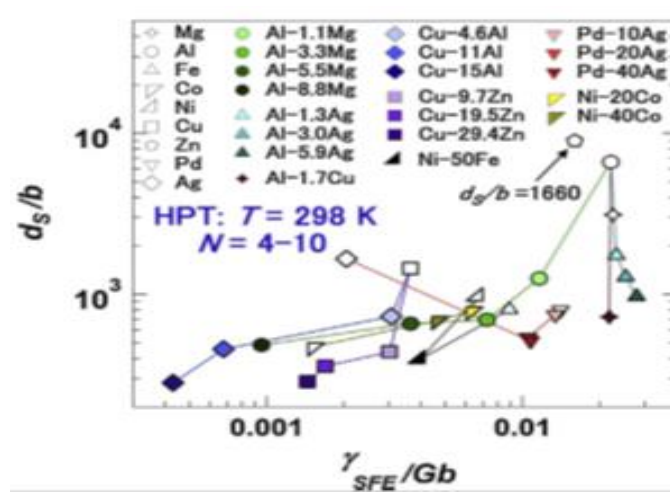

Fig. 5.4.Plots of ds/b v/s SFE/Gb [16]

The hardness values after HPT processing with increasing alloying content in two alloy systems viz. Ni-Fe and Ni-Co of various composition across the disk at N=10

is shown in Fig.5.5. It is clearly observed from the graph with the increase in solute concentration hardness increases in both the alloys. It can also be observed that there is not much difference in the hardness values of Ni-20%Fe and Ni-30%Fe, but homogeneity in hardness is achieved only in Ni-30%Fe and Ni-60%Co. This increase in hardness is due to solid solution hardening as well as due to effect of decrease in grain size. Hardness values of Ni-20%Fe and Ni-30%Fe are higher than that of Ni-60%Co. These greater hardness may be attributed to solution hardening effect which is pronounced in Ni-Fe alloys but not in Ni-Co alloys. Recently a study on various FCC alloys deformed by HPT has been carried out and it has been reported that decrease in grain size is more important hardening mechanism in single phase alloys whereas effect of solid solution hardening is less than 15% of total hardening [18].
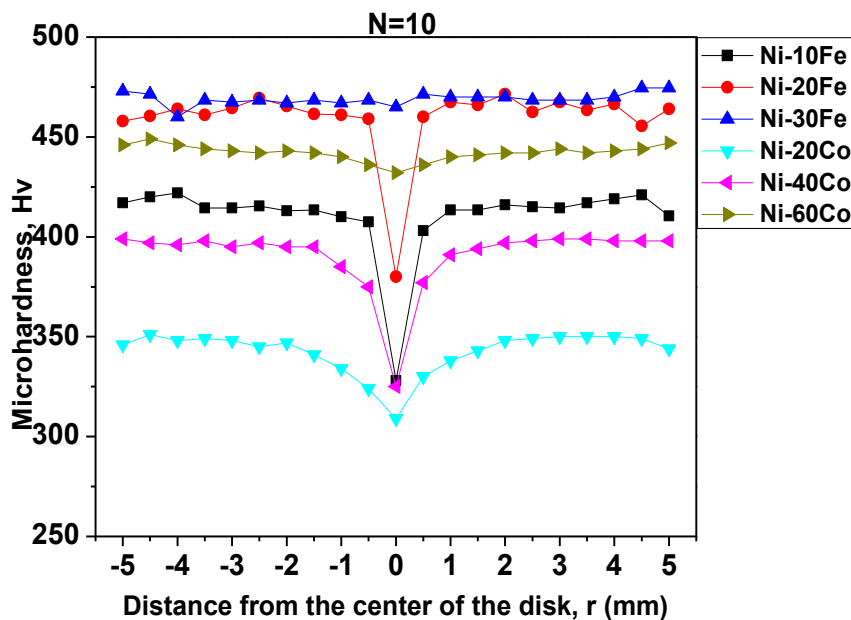

Fig 5.5.Hardness evolution plot across the disk of Ni-10%Fe, Ni-20%Fe and Ni-30%Fe at N=10

5.2. Evolution of Texture

SFE plays an important role on the development of texture during plastic deformation [21]. Since by alloying Ni with Fe there is not any significant change in SFE, thus, we can assume that texture development of Ni-Fe alloys can be very similar to pure Ni. The development of texture in HPT processed Ni-Fe alloys shows the presence of all the conventional texture components during simple shear [22,23]. The trend followed by various texture components with varying strain values remains almost similar with increasing alloying content in Ni-Fe alloys i.e. the volume fraction of a texture component at particular strains does not differ much in all the three Ni-Fe alloys, as shown in Fig.5.6, which may be attributed to almost similar SFE of all three Ni-Fe alloys considered. This dependence of texture on SFE can be contrasted with Ni-Co alloys in which SFE decreases drastically on Co addition. In Ni-Co alloys the volume fraction of various texture components is different at particular strain value in various Ni-Co alloys as shown in Fig.5.7.
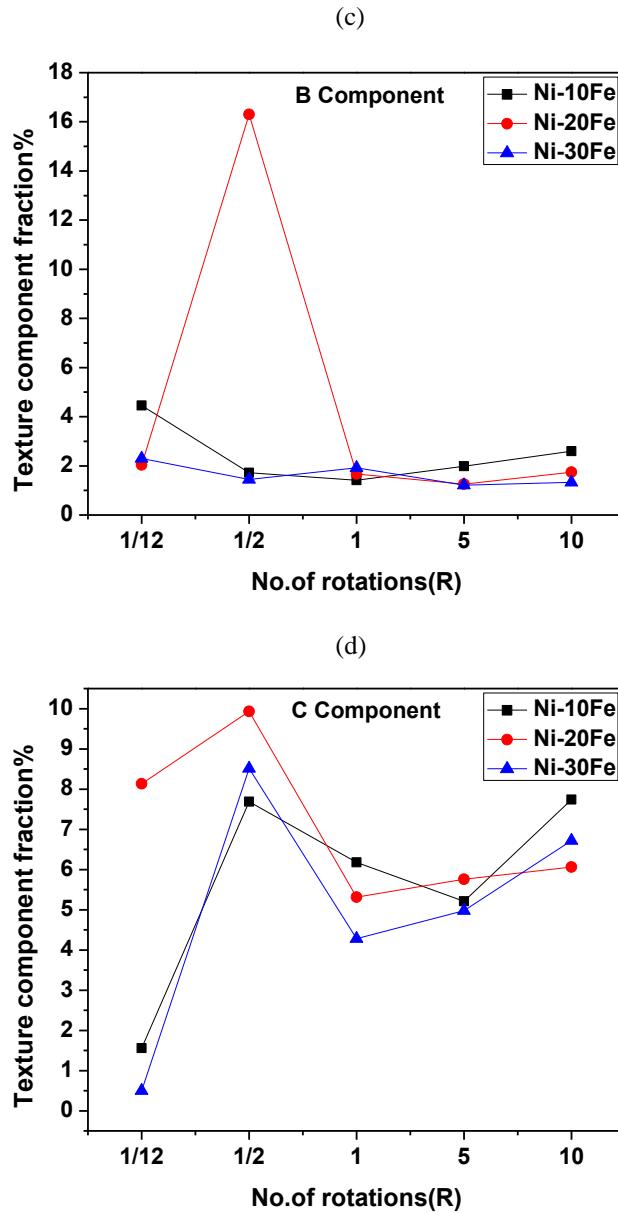
(a)

(b)

43

(c)

(d)
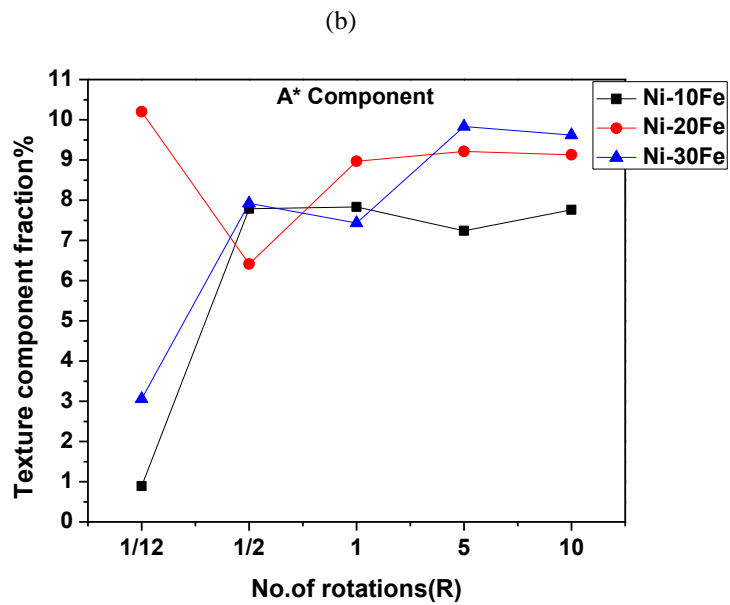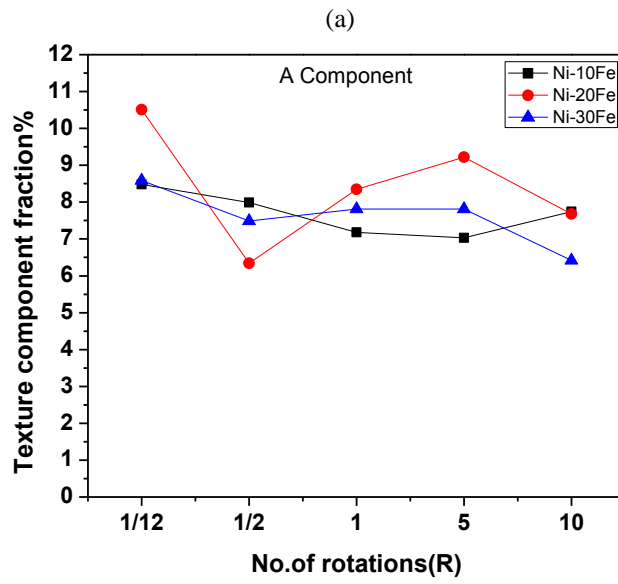
Fig.5.6.Volume fractions of the texture components with increasing number of rotations of the HPT Processed three Ni-Fe alloys: (a) A/A-, (b) A*-components, (c) B/B- components (d) C-component

Contrasting Ni-Fe alloys with Ni-Co alloys we can observe that A, A*, B and C are prominent texture components in both the alloys. In both the alloy systems A, A* and C components are strong components, B component is weak and volume

fraction is similar at all strain values. C component decreases with increasing Co content and increasing strain but in Ni-Fe alloys it increases till equivalent strain of ~3 thereafter it decreases and increases periodically.
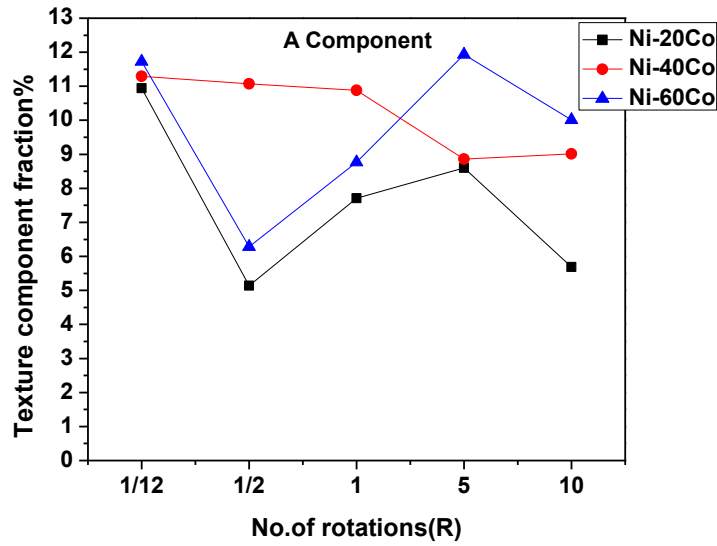
(a)

(b)

(c)

(d)
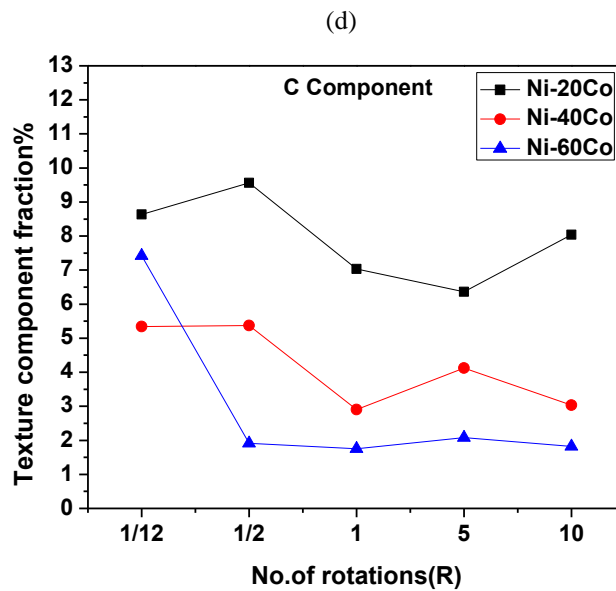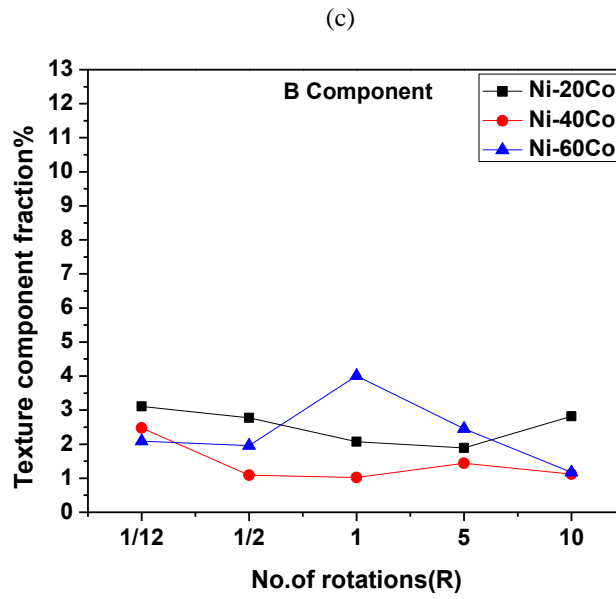
Fig.5.7.Volume fractions of the texture components with increasing number of rotations of the HPT Processed three Ni-Co alloys: (a) A/A-, (b) A*-components, (c) B/B- components (d) C-component
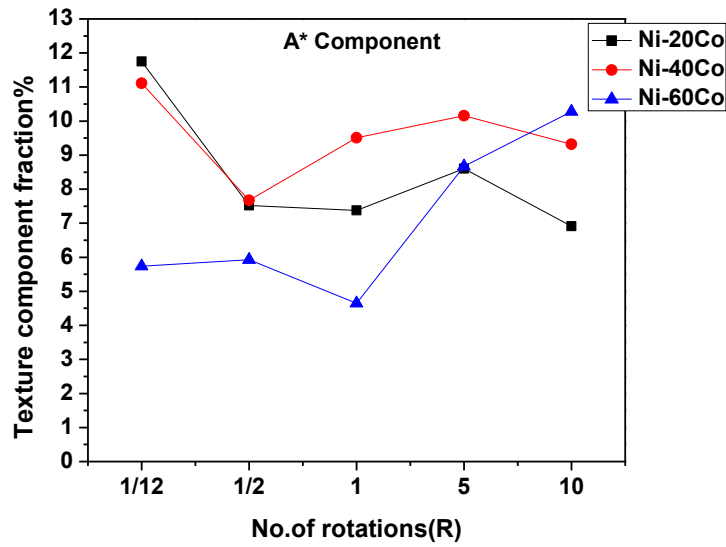
Apart from the ideal shear component, {112}<11-1> component is present predominantly in both the alloys. The volume fraction of this component increases with increasing strain values although this increase is far more in Ni-Fe as compared

with Ni-Co. It can be observed from Fig.5.8(a) that volume fraction of this component also increases with increasing alloying content in Ni-Fe alloys.

(a)

(b)
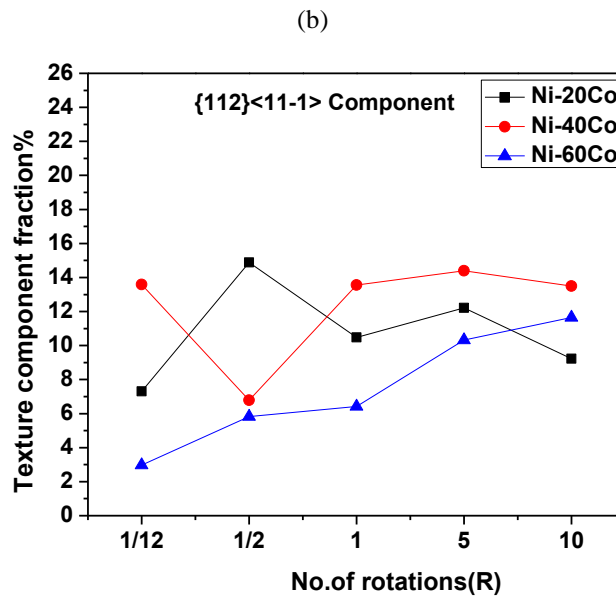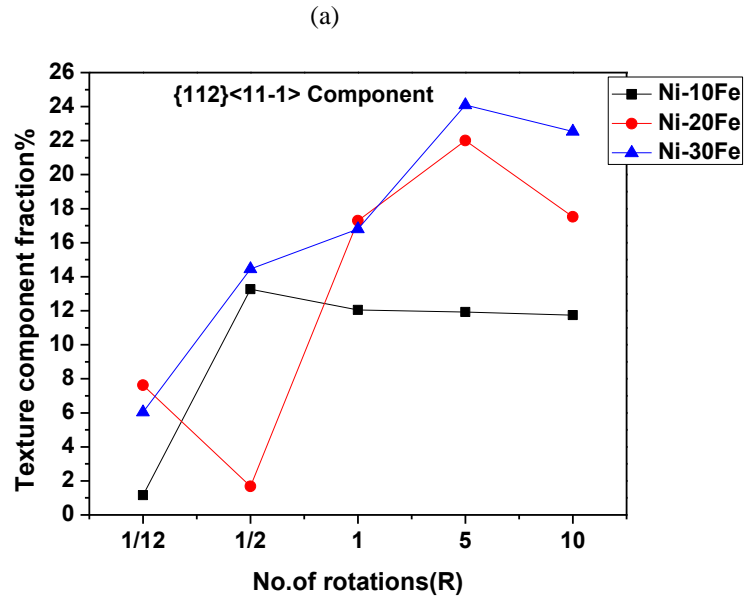
Fig.5.8.Volume fraction of {112}<11-1> texture components at edge regions for different numbers of rotations in various (a)Ni-Fe, (b)Ni-Co alloys

Observing pole figures and ODF of various Ni-Fe alloys at various strain values at the edge region in Fig.4.12 and Fig.4.13, we can see that at high strain values,

there is hardly any change in texture of Ni-10%Fe, Ni-20%Fe and Ni-30%Fe apart

from the fact that with increasing alloying some texture strengthening is observed.

This can be attributed to similar SFE in Ni-Fe alloys.

Chapter 6

Summary and Conclusion

The main conclusions that may be drawn from the present study are:

1. Grain size is smaller at the edge region than in the central region at lower number of rotations in the three alloys. As the number of rotations is increased grain size becomes homogenous throughout the disk. Extreme homogeneity in terms of grain size is achieved in Ni-20%Fe and Ni-30%Fe is at N=10.

2. Although there is no significant change in SFE with alloying Ni with Fe, but the grain size achieved is comparable to the alloys having very low SFE, this suggests that solute effect is equally effective in grain refinement as SFE.

3. As the number of turns increase hardness value increases in the three alloys, however, there is no significant increase in hardness after one complete rotation.

4. Hardness values as compared with low SFE alloys, such as, Ni-Co is considerably higher in Ni-Fe alloys despite having almost similar grain size which implies that increases hardness is due to solution hardening.

5. Texture evolution in the three alloys is similar. A, A* and C components are having higher volume fractions while B has minor presence. In all the three alloys {112}<11-1> component is dominating and the volume fraction of this component increases with increasing alloying addition.

References

[1] R. Z. Valiev, Y.Estrin, Z.Horita, T. G. Langdon, M. J. Zehetbauer, and Y. T. Zhu. Producing bulk ultrafine grained materials by severe plastic deformation.JOM, (2006) 33-39.

[2] A. P.Zhilyaev, T.G.Langdon.Using high-pressure torsion for metal processing: Fundamentals and applications.Progress in Materials Science 53, (2008) 893‑979.

[3] R.Z. Valiev, R. K. Islamgaliev, I. V. Alexandrov.Bulk nanostructured materials from severe plastic deformation.Progress in Materials Science 45, (2000) 103-189.

[4] A. Azushima, R. Kopp, A. Korhonen, D.Y. Yang, F. Micari, G.D. Lahoti , P. Groche, J. Yanagimoto, N. Tsuji, A. Rosochowski, A. Yanagida. Severe plastic deformation (SPD) processes for metals. CIRP Annals - Manufacturing Technology 57, (2008) 716‑735.

[5] R.Pippan, F.Wetscher, M. Hafok, A.VorhauerI.Sabirov. The limits of refinements by severe plastic deformation.Advanced engineering materials, (2006) 1046-1056.

[6] K. J. Al-Fadhalah, S. N. Alhajeri, A. I. Almazrouee, T. G. Langdon.Microstructure and microtexture in pure copper processed by high-pressure torsion. J. Mater Sci., (2013).

[7] R.K.Ray. Rolling texture o pure Nickel, Nickel-Iron and Nickel-Cobalt alloys. Acta Metall. Mater 43, (1994) 3861-3872.

[8] M. A. Meyers, K.K. Chawla, Mechanical behavior of materials, Prentice-Hall. (1999).

[9] D. J. Siegel. Generalized stacking fault energies, ductilitiesand twinnabilities of Ni and selected Ni Alloys. Applied Physics Letters 87, (2005).

[10] Y.H.Zhao, X.Z.Liao, Y.T. Zhu, Z. Horita, T.G. Langdon. Influence of stacking fault energy on nanostructure formation under highpressure torsion. Materials Science and Engineering A 410–411 (2005) 188–193.

[11] P. Zhang, X.H. An, Z.J. Zhang, S.D. Wu, S.X. Li, Z.F. Zhang, R.B. Figueiredo, N. Gao T.G. Langdon. Optimizing strength and ductility of Cu-Zn alloys through severe plastic deformation. ScriptaMaterialia, (2012).

[12] X.H.An,Q.Y Lin, S.D. Wu, Z.F. Zhang, R.B.Figueiredo, N. GaoT.G. Langdon. The influence of stacking fault energy on the mechanical properties of nanostructured Cu and Cu–Al alloys processed by high-pressure torsion.ScriptaMaterialia 64, (2011) 954-957.

[13] P.L. Sun,Y.H. Zhao, J.C. Cooley, M.E. Kassner, Z. Horita, T.G. Langdon, E.J. Lavernia, Y.T. Zhu. Effect of stacking fault energy on strength and ductility of nanostructured alloys:An evaluation with minimum solution hardening. Materials Science and Engineering A 525, (2009) 83–86.

[14] D.Orlov, P. P. Bhattacharjee, Y. Todaka, M. UmemotoN. Tsuji. Texture evolution in pure aluminum subjected to monotonous and reversal straining in high pressure torsion. ScriptaMaterialia 60, (2009) 893-896.

[15] A. Loucif, T. Baudin, F. Brisset, R. B. Figueiredo, R. Chemam T.G. Langdon.An investigation of microtexture evolution in an AlMgSi alloy processed by high-pressure torsion. Materials Science Forum 702-703, (2012) 165-168.

[16] H.W. Zhang, X. Huang, N. Hansen. Evolution of microstructural parameters and flow stresses toward limits in nickel deformed to ultra-high strains. ActaMaterialia 56, (2008) 5451–5465.

[17] D.A.Hughes, N. Hansen, High angle boundaries formed by grain subdivision mechanisms. ActaMaterialia, 45 (1997) 3871-3886.

[18] K. Edalati, D. Akama, A. Nishio, S. Lee, Y.Yonenaga, J. M. Cubero-Sesin, Z. Horita. Influence of dislocation–solute atom interactions and stacking fault energy on grain size of single-phase alloys after severe plastic deformation using high-pressure torsion. ActaMaterialia 69, (2014) 68–77.

[19] C. Elango. Effect of Stacking Fault Energy on Microstructure and Texture Evolution in Ni-Co Alloys during Severe Plastic Deformation by High Pressure Torsion. M. Tech Thesis, IIT Hyderabad, (2013).

[20] Y.B.Wang, X.Z. Liao, Y.H. Zhao, E.J. Lavernia, S.P. Ringer, Z. Horita, T.G. Langdon. The role of stacking faults and twin boundaries in grain refinement of a Cu-Zn alloy processed by high-pressure torsion. Materials Science and Engineering: A. 527 (2010) 4959-4966.

[21]D. A. Hughes, R. A. Lebensohn, H. R.Wenk A. Kumar. Stacking fault energy and microstructure effects on torsion texture evolution. Proc. R. Soc. Lond. A (2000) 921-953.

[22]F. Montheillet, M. Cohen, J. J. Jonas, Axial stresses and texture development during the torsion testing of Al, Cu and α-Fe. ActaMetallurgica 32 (1984) 2077-2089.

[23] G. R.Canova, F.Kocks, J. J.Jonas, Theory of torsion texture development. ActaMetallurgica 32 (1984) 211-226.

[24]P. C. J.Gallagher, The Influence of Alloying, Temperature, and Related Effects of the Stacking Fault Energy Metallurgical Transactions1, (1970) 2429.

[25]R. E. Schramm and R. P. Reed, Stacking Fault Energies of FCC Fe-Ni Alloys byX-Ray diffraction line profile analysis. Metallurgical Transactions A, (1976) 359.